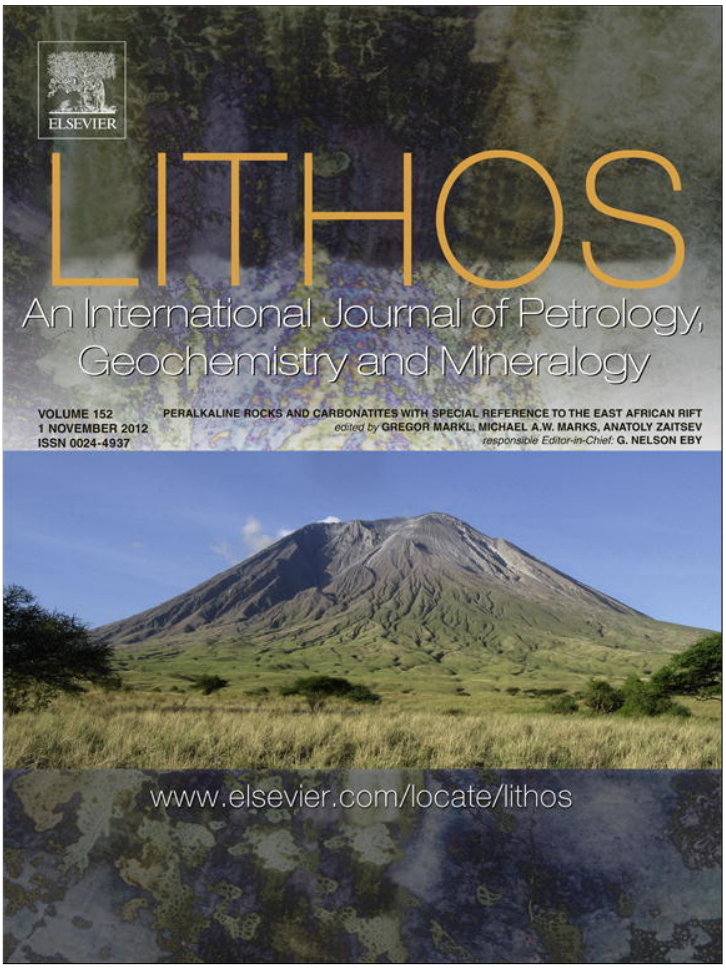

Lithos 152 (2012) 66–83

Contents lists available at SciVerse ScienceDirect

Lithos

journal homepage: www.elsevier.com/locate/lithos

Mineralogy, geochemistry and petrology of the phonolitic to nephelinitic Sadiman volcano, Crater Highlands, Tanzania

A.N. Zaitsev [a,b,*], M.A.W. Marks [c], T. Wenzel [c], J. Spratt [b], V.V. Sharygin [d], S. Strekopytov [b], G. Markl [c]

[a] Department of Mineralogy, Faculty of Geology, St. Petersburg State University, University Emb. 7/9, St. Petersburg, 199034, Russia
[b] Department of Mineralogy, Natural History Museum, Cromwell Road, London, SW7 5BD, UK
[c] Universität Tübingen, Mathematisch-Naturwissenschaftliche Fakultät, FB Geowissenschaften, Wilhelmstrasse 56, D-72074 Tübingen, Germany
[d] V.S. Sobolev Institute of Geology and Mineralogy, Siberian Branch of Russian Academy of Sciences, Koptuga pr. 3, Novosibirsk, 630090, Russia

ARTICLE INFO

Article history:
Received 12 October 2011
Accepted 1 March 2012
Available online 9 March 2012

Keywords:
Nephelinite
Phonolite
Mineral composition
Melt inclusions
Mineral stability fields
Sadiman volcano

ABSTRACT

Sadiman volcano is located in the Crater Highlands area of northern Tanzania, which lies next to the western escarpment of the Gregory rift—a part of the eastern branch of the East African Rift system. It consists of interlayered phonolitic tuffs, tuff breccias (with blocks of nephelinites) and nephelinitic lava flows. Rare xenoliths of phonolite lava and ijolite were observed within the nephelinite lavas with ijolite blocks occurring in phonolitic tuffs. No evidence for the presence of melilite-bearing and/or carbonatitic rocks was found during this study. On the basis of petrography, mineralogy and geochemistry the nephelinites are divided into highly porphyritic nephelinite, wollastonite nephelinite and phonolitic nephelinite, the latter of which is the dominant variety at Sadiman. Nepheline + clinopyroxene + titanite ± perovskite ± andradite–schorlomite ± wollastonite ± sanidine ± sodalite are the principle pheno- and microphenocryst phases. The nephelinites are highly evolved (Mg# = 0.17–0.26) alkaline to peralkaline (AI = 0.88–1.21) rocks enriched in incompatible elements such as Rb, Ba, Th, U, Nb, Pb, Ta, Sr and light REEs, and strongly depleted in P and Ti. This suggests derivation from an enriched mantle source and fractionation of apatite and Ti-rich mineral(s). Primary melt inclusions in nepheline phenocrysts ($T_{homogenization}$ = 860–1100 °C) indicate enrichment of volatile components in the melts, particularly of fluorine (up to 1.8 wt.% in silicate glass) resulting in the formation of daughter fluorite in partly and complete crystallized inclusions. The Sadiman nephelinites crystallized under relatively oxidizing conditions (above the FMQ buffer), which differ from the reducing conditions reported for trachytic and pantelleritic rocks from other parts of the Gregory rift. Similar rock types and relatively oxidizing conditions are known from Oldoinyo Lengai and other localities, all of which are closely associated with carbonatites. By analogy, we conclude that andradite–schorlomite-rich nephelinites may indicate a pre-stage on the evolutionary path towards carbonatitic magmatism.

1. Introduction

Sadiman volcano (3°11′S, 35°25′E), also known as Satiman, is part of the Neogene–Quaternary volcanic complexes forming the Crater Highlands area in northern Tanzania (Fig. 1a) (Dawson, 2008). This area lies next to the western escarpment of the Gregory rift which is part of the eastern branch of the East African Rift System. The Crater Highlands, also termed as the Ngorongoro Volcanic Highlands, consist of several large volcanic complexes including the 2.4–2.2 Ma Lemagarut and the 2.25–2.0 Ma Ngorongoro basalt–trachybasalt–trachyandesite volcanoes (Ngorongoro also contains trachydacite) as well as the 1.6–1.5 Ma Oldeani basalt–trachyandesite volcano (Dawson, 2008; Mollel et al., 2008; 2011).

Sadiman is a highly eroded high stratovolcano whose top lies at 2870 m above see level, rising for about 400–500 m above the Malanja depression. It is located between Lemagarut, Oldeani and Ngorongoro (Fig. 1a). The volcano is well known having been previously cited as the source of the Laetoli Footprint Tuff, where 3.66 Ma *Australopithecus afarensis* footprints were discovered in 1976 (Harrison, 2011a; Leakey and Hay, 1979). However, it has recently been suggested that available geological, mineralogical and geochemical data for the Sadiman volcano do not currently support this hypothesis (Zaitsev et al., 2011). Sadiman is also believed to be a source of the Wembere-Manonga sediments (Manonga Valley), located about 170 km southwest of Laetoli (Harrison, 2011b; Mollel et al., 2011; Mutakyahwa, 1997).

In this paper we report new data from 28 samples of Sadiman lavas, tuffs and epiclastic rocks from (i) east and summit ridge outcrops, (ii) a stream channel and outcrops at the base of the north side of the volcano (Fig. 1b), and (iii) unspecified localities within Sadiman (Belousov et al., 1974). The major goals of this study are to

* Corresponding author at: Department of Mineralogy, Faculty of Geology, St. Petersburg State University, University Emb. 7/9, St. Petersburg, 199034, Russia. Tel.: +7 812 3289481.
E-mail address: burbankite@gmail.com (A.N. Zaitsev).

0024-4937/$ – see front matter © 2012 Elsevier B.V. All rights reserved.
doi:10.1016/j.lithos.2012.03.001

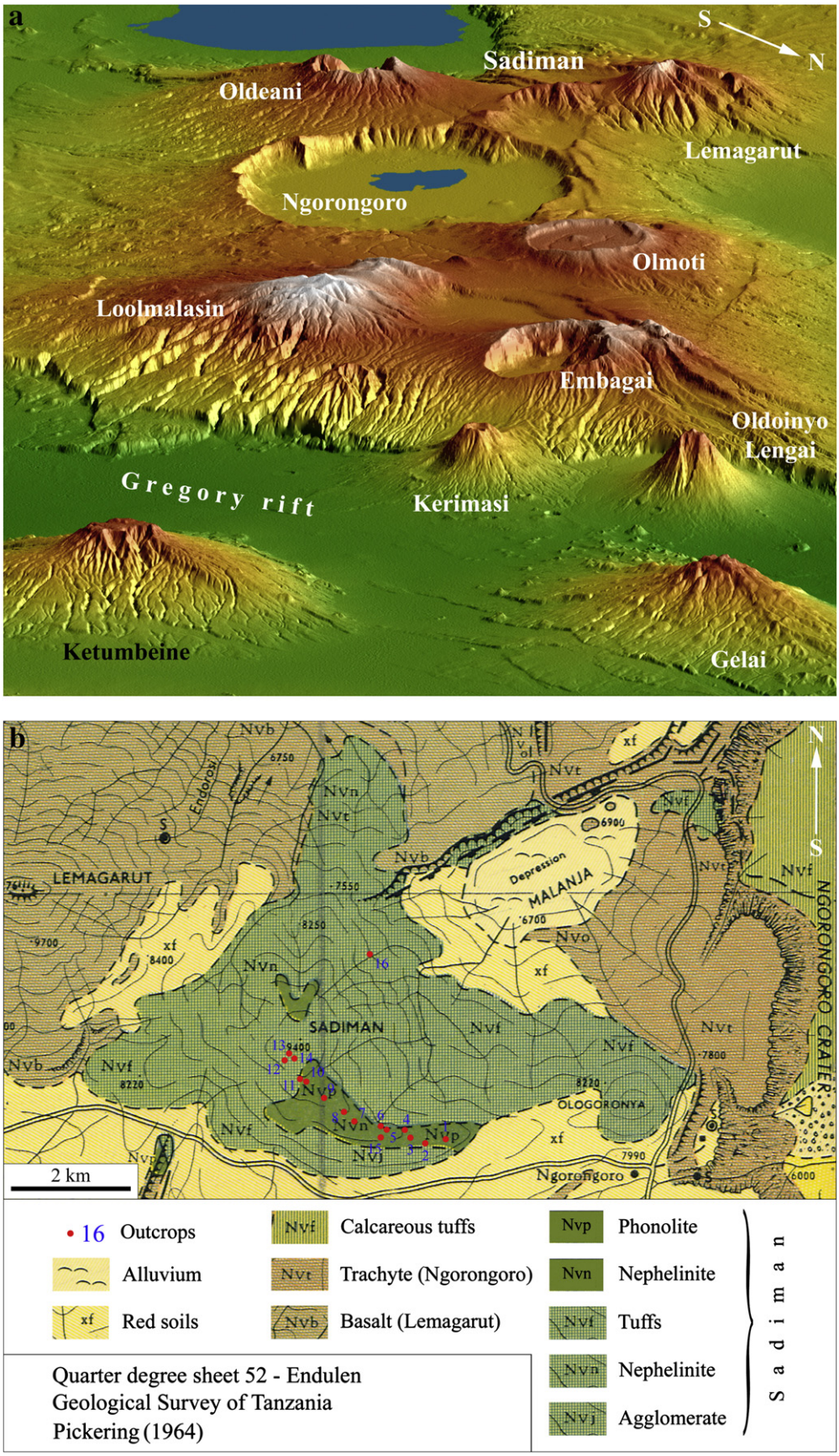

Fig. 1. (a) Volcanoes in the Crater Highlands area and the Gregory rift in northern Tanzania. SRTM data (February 2000); view size: 44.5 km wide by 142.5 km distance; location: 3° South latitude, 36° East longitude; orientation: View 35° south of west, 15° below horizontal; image courtesy NASA/JPL/NGA Shuttle Radar Topography team. (b) Pickering's (1964) geological map of Sadiman volcano, with lithologies as identified by Pickering. Abbreviations: Nv = Neogene volcanic rocks, f = tuffs, t = trachyte, b = basalt, p = phonolite, n = nephelinite, j = agglomerate Numbered outcrops (red dots) represent samples collected for the current study.

(1) evaluate the occurrence of various rock types at Sadiman, (2) establish a detailed mineralogical and geochemical characterization of the Sadiman rocks, and (3) constrain the petrological evolution of the nephelinites based on intensive parameters such as temperature, silica activity (a_{SiO_2}) and oxygen fugacity (f_{O_2}).

2. Geological background

Sadiman is a highly vegetated, poorly exposed volcano and only a limited number of outcrops are known, e.g. six outcrops have been identified by Mollel et al. (2011) whereas sixteen outcrops have been mapped in this study. According to Pickering's (1964) QDS 52 "Endulen" map (Fig. 1b) "Sadiman … made up largely of nephelinitic tuffs and agglomerates with subsidiary lava flows. Nephelinites and phonolites cap a prominent ridge on the south-east side of the volcano". Pebbles, cobbles and boulders of nephelinite, phonolite and ijolite have been reported from stream deposits on the north slope of the volcano (Hay, 1976). The occurrence of nephelinites at Sadiman has been confirmed by whole rock and mineral analyses of Paslick et al. (1995) and by a recent study of the Sadiman lavas by Mollel et al. (2011). Geochemical data given by Mollel et al. (2011) support the occurrence of phonolite at Sadiman, however, the mineralogical description of the studied rocks indicates that they lack alkali feldspar (sadinine) in two of three "phonolite" samples. Direct evidence for the presence of phonolites at Sadiman was given by Zaitsev et al. (2011), who reported them as small xenoliths in nephelinite, but no phonolite lava flows have been identified yet.

Published data and our field observations suggest that Sadiman volcano consists of interlayered massive phonolitic tuffs, tuff breccias (with blocks of nephelinites) and nephelinite lava flows with phonolite tuff xenoliths. Unfortunately, the scarcity of outcrops makes it impossible to estimate the relative proportions of extrusive and effusive rocks at Sadiman. Ijolite (a plutonic nepheline–clinopyroxene rock) xenoliths were observed in nephelinite lavas and phonolite tuffs located on the east ridge of the volcano. The volcano is covered by loose reddish to brownish phonolitic tuffs with numerous rounded blocks of nephelinites.

The geological and mineralogical study of the Laetoli tuffs, located about 20 km east of Sadiman, by Hay (1978) leads to an assumption that carbonatitic and melilititic rocks could occur at Sadiman (Hay, 1987). The presence of melilite nephelinite, phonolitic trachyte and sodalite phonolite at Sadiman was also suggested by Woolley (2001) and carbonatite and melilitite were also mentioned by Dawson (2008). However, these rocks have never been described from the volcano.

Geochronological data indicate that Sadiman is the oldest extinct volcano in the Crater Highlands. The first published K–Ar ages obtained from nephelinite lavas show a wide range from 4.5 Ma (Bagdasaryan et al., 1973) to 3.7 Ma (Hay, 1976), and a younger age of 3.3 Ma was reported by P.C. Manega (Foster et al., 1997). Recent $^{40}Ar/^{39}Ar$ dating of two nephelinite and one phonolite sample by Mollel et al. (2011) suggested that Sadiman was active between 4.6 and 4.0 Ma, with a possible older age of 4.8 Ma. All available age data indicate a duration of Sadiman activity for about 1.5 Ma, much longer than the other volcanoes in the Crater Highlands (Mollel et al., 2008, 2011). Clearly, a further geochronological study is needed, particularly to confirm Sadiman eruptions between 4.0 and 3.3 Ma.

3. Analytical methods

Polished thin sections of lavas and tuffs and epoxi blocks with fractions of heavy minerals were studied using scanning electron microscopy (SEM—JEOL 5900LV) and energy-dispersive X-ray microanalysis (EDX—Oxford instruments INCA) at the Natural History Museum (NHM), London. SEM and EDX were also used for the study of sodalite. Wavelength-dispersive electron probe microanalyses (WD-EPMA) of major, minor and accessory minerals were obtained using a JEOL 8900 Superprobe at Tübingen University (TU) (nepheline, clinopyroxene, sanidine, anorthoclase, wollastonite, aenigmatite, magnetite, ilmenite and pyrrhotite), and a Cameca SX-100 electron microprobe at the NHM (perovskite, andradite, schorlomite, titanite and magnetite) (for analytical details see Supplementary text).

Bulk contents of major and minor elements including F, Cl and S were determined from whole rock pressed powders by X-ray fluorescence (XRF, Bruker AXS S4 Pioneer) at TU. Mean detection limits for F, Cl and S were around 50, 50 and 10 ppm, respectively. The average errors of the F, Cl and S determinations in our samples were around 30, 20 and 10 ppm, respectively. Trace elements including REEs were determined after open acid digestion ($HF + HNO_3 + HClO_4$) by quadrupole inductively coupled plasma mass-spectrometry (ICP-MS) (Varian 810) and (Sr and Ba only) by inductively couple plasma atomic emission spectroscopy (ICP-AES) (Varian Vista-Pro Axial) at the NHM. Further details of sample preparation and the ICP-MS analysis including a correction for polyatomic interferences (Eu, Gd, Tb, Hf and W) can be found in Ferrat et al. (2012) and Hezel et al. (2011). Analytical accuracy was checked by comparison to the USGS standard rocks AGV-1 (andesite) and BCR-1 (basalt) and was found to be within ±7% for all REEs and most other elements.

The melt inclusion study was performed at V.S. Sobolev Institute of Geology and Mineralogy (IGM), Novosibirsk. The Vernadsky high-temperature heating stage (Sobolev and Slutsky, 1984) was used for heating experiments with melt inclusions in phenocrystic minerals. The chemical composition of unheated inclusions (glass + daughter phases) in nepheline was analyzed by WD-EPMA using a Camebax 50× electron microprobe (for analytical details see Supplementary text).

4. Petrography and mineral chemistry

Our field data, optical petrography and electron microscopy studies show that nephelinites are the major effusive rocks at Sadiman volcano; phonolite lavas were observed only as small xenoliths (<1 cm in size) in the nephelinites (Zaitsev et al., 2011). Nephelinites range from phenocryst-poor to phenocryst-rich rocks with crystalline groundmass, and phonolites are phenocryst-rich rocks. Rarely, nephelinites contain xenoliths of annite-bearing ijolite (0.5–25 cm in size).

On the basis of their texture, structure and mineralogy the Sadiman nephelinites are divided into four types: Nephelinite I (relatively rare type—observed from one lava flow and blocks in tuffs; it is a phenocryst-rich rock with only a small proportion of groundmass), nephelinite II (very rare type—observed from one lava flow, with wollastonite as one of the phenocryst minerals), nephelinite III (common rock type occurring as lava flows and blocks in tuffs) and nephelinite IV (also a common rock type occurring as lava flows and blocks in tuffs) (Fig. 2) (Table 1). Both nephelinite types III and IV contain sanidine as a groundmass mineral, but nephelinite III contains Ti-rich minerals (schorlomite and perovskite) as pheno- and microphenocrysts, while these are absent from nephelinite IV. In total, 25 minerals have been identified in the nephelinites during this study, 19 of which were previously unknown from the Sadiman rocks (Mollel et al., 2011; Paslick et al., 1996). Note that the mineral list in Table 1 does not include low-temperature secondary minerals.

In contrast, phonolite from Sadiman is mineralogically very simple and contains sanidine–anorthoclase, nepheline, diopside–hedenbergite, titanite, apatite and magnetite (the term phonolite is used here according to the mineralogical definition of IUGS as a volcanic rock consisting essentially of alkali feldspar and any foids). Selected analyses of the major minerals from the Sadiman nephelinites and phonolites are given in Table 2 and additional data on mineral chemistry are given in Supplementary Tables 6–17.

Nepheline occurs in all studied samples as phenocrysts and within the groundmass. Euhedral phenocrysts reach up to 12×8 mm in size (Fig. 2). In nephelinites the mineral shows a wide range in potassium content, from 8.2 wt.% K_2O (1.02 apfu (atoms per formula

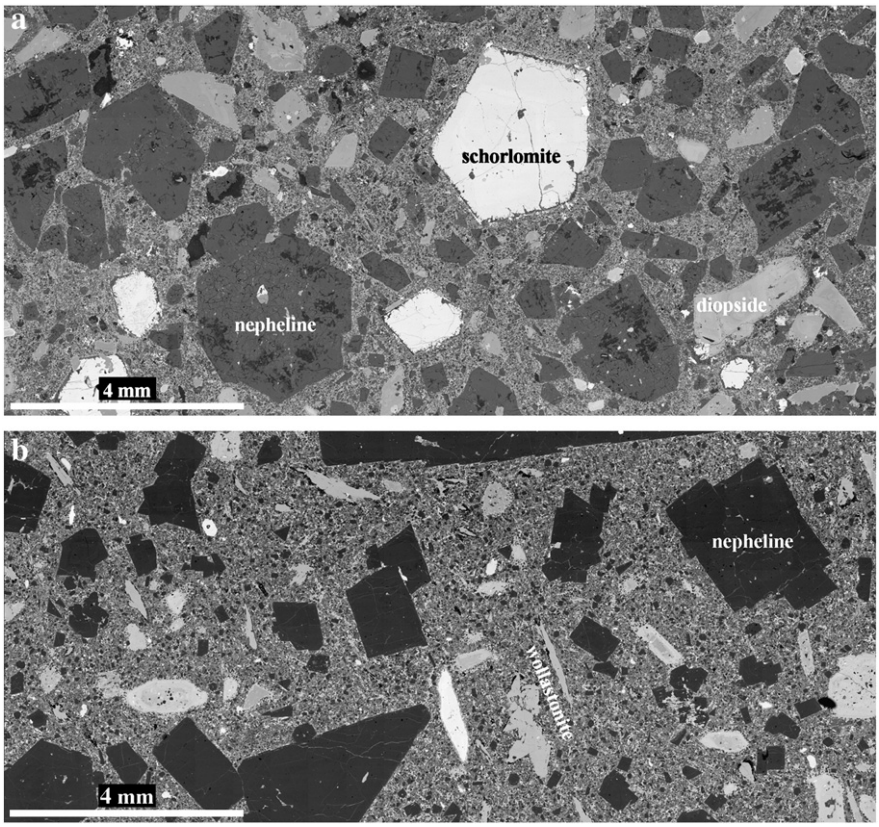

Fig. 2. Back-scattered electron (BSE) images of (a) nephelinite I, sample SAD 10 and (b) nephelinite II, sample SAD 11.

unit)) in nephelinite I to 3.4 wt.% K_2O (0.42 apfu) in nephelinite III. Minor elements are Fe (0.5–2.1 wt.% Fe_2O_3) and Ca (<0.5 wt.% CaO). Nepheline from the phonolite is characterized by lower potassium contents (2.1 to 2.9 wt.% K_2O, 0.25–0.36 apfu), 1.0–1.3 wt.% Fe_2O_3 and 0.3 wt.% CaO (Table 2, Supplementary Table 6). On the Hamilton plot (Fig. 3) data points from nephelinites form a broad field ($Ne_{71-83}Ks_{10-26}Qz_{0-9}$) and data points from phonolites have a distinct composition ($Ne_{78-83}Ks_{6-9}Qz_{7-14}$) compared to nephelinites.

Clinopyroxene occurs as phenocrysts, microphenocrysts, and microlaths (Fig. 2) in nephelinites and phonolites. Mineral formulae show that clinopyroxene is essentially of the diopside–hedenbergite solid solution series, with appreciable amounts of an aegirine component present only in the nephelinites (Figs. 4–5, Table 2, Supplementary Table 7). Petrographic observations and electron microscopy suggest the presence of at least three distinct crystal types among pyroxene phenocrysts in the nephelinites. Type 1 pyroxenes have a relatively aegirine- and hedenbergite-rich green core (Aeg = 15–23 mol%, Hd = 38–43 mol% and Di = 32–35 mol%), which transforms to a diopside-rich zone (Aeg = 5–9 mol%, Hd = 13–34 mol% and Di = 38–51 mol%) between core and mantle (Fig. 4a). Type 2 pyroxenes have a diopside-rich core (Aeg = 5–9 mol%, Hd = 19–34 mol% and Di = 49–64 mol%) and a hedenbergite-rich rim (Aeg = 9–12 mol%, Hd = 38–49 mol% and Di = 33–46 mol%) (Fig. 4b). Type 3 pyroxenes are oscillatory zoned (Fig. 4c). For the first and second types, the crystal cores show resorption, as is typical for pyroxene in alkaline rocks, and are commonly not in optical continuity with the rim. The outermost rims for all three types are relatively diopside-poor with hedenbergite and aegirine as the dominant components. The composition of the microphenocrysts is similar to that of mantle and rim zones of the phenocrysts and corresponds to a diopside–hedenbergite solid solution. Aegirine-augite (with up to 49 mol% of the aegirine end member) forms distinct narrow rims on pheno- and microphenocrysts and occurs interstitially within the groundmass. Phonolite pyroxene (microphenocrysts and rarely phenocrysts) falls within a diopside–hedenbergite solid solution (Supplementary Table 7). The compositional evolution of the pyroxene from diopside to hedenbergite and aegirine-augite is shown on the ternary plot Na–Mg–Fe^{2+} + Mn (Fig. 5). Minor elements present within the pyroxenes are Al (0.2–4.5 wt.% Al_2O_3), Ti (0.3–2.3 wt.% TiO_2), Mn (0.1–0.7 wt.% MnO) with Zr as a trace element (<0.1 wt.% ZrO_2). Mineral formulae show that all Al is present in the tetrahedral site (Supplementary Table 7).

Garnet occurs in nephelinites I, II and III and forms euhedral crystals of up to 4 mm in diameter (Fig. 2a), and occasionally, it contains replacement relics of titanite (Fig. 6a). Some crystals show replacement by an unidentified hydrous(?) aluminosilicate of Ca, Na and K, götzenite and/or barytolamprophyllite (Fig. 6a). All crystals exhibit internal growth zonation. Recalculation of analyses on the basis of 12 oxygens and 8 cations shows that garnet is rich in Fe^{3+} and Ti and belongs to the andradite–schorlomite solid solution series with cation variations for the *Y* site between ($Fe^{3+}_{1.01}Ti_{0.68}Fe^{2+}_{0.25}others_{0.06}$) and ($Fe^{3+}_{0.43}$ $Ti_{1.14}Fe^{2+}_{0.28}others_{0.15}$) (Table 2, Supplementary Table 8, Fig. 6b). The *Z* site contains 0.07–0.23 Al apfu and 0.16–0.54 Fe^{3+} apfu. Andradite occurs in nephelinite II. Andradite and schorlomite are typical for nephelinites I and III, although some samples of nephelinites I and III contain only schorlomite. An exception is garnet occurring as reaction rims around titanite—it is strongly enriched in Ti (21.1–21.7 wt.% TiO_2—1.34–1.38 apfu) and contains significant Fe^{2+} compared to Fe^{3+} (0.41–0.46 and 0.06–0.13 apfu, respectively). This mineral is chemically similar to the garnet end-member morimotoite (Supplementary Table 8). Minor and trace elements include Mg (0.3–1.1 wt.% MgO), V (0.1–0.6 wt.% V_2O_3), Na (0.1–0.5 wt.% Na_2O), Zr (0.2–0.4 wt.% ZrO_2), Nb (≤0.2 wt.% Nb_2O_5) and Y (≤0.1 wt.% Y_2O_3).

Wollastonite occurs in nephelinite II as pheno- and microphenocrysts (Fig. 2b), and was observed as rare tiny inclusions in garnet phenocrysts in nephelinite I. Nearly all wollastonite crystals have a reaction rim consisting of an unidentified K–Mg–Al–Ca silicate. The mineral contains minor Fe (1.0–1.1 wt.% FeO) and traces of Mn (≤0.4 wt.% MnO) and Mg and Na (≤0.1 wt.% oxides) (Supplementary Table 9).

Table 1
Mineralogy of the Sadiman nephelinites.

Rock type	I	II	III	IV
Phenocrysts	Nepheline	Nepheline	Nepheline	Nepheline
	Clinopyroxene	Clinopyroxene	Clinopyroxene	Clinopyroxene
	Garnet	Garnet	Garnet	
	Perovskite		Perovskite	
		Wollastonite		
	Titanite	Titanite	Titanite	Titanite
	Apatite	Apatite		
Microphenocrysts	Clinopyroxene	Clinopyroxene	Clinopyroxene	Clinopyroxene
	Nepheline	Nepheline	Nepheline	Nepheline
		Wollastonite		
			Sanidine	Sanidine
	Titanite	Titanite	Titanite	Titanite
		Potassicarfvedsonite		
	Garnet	Garnet	Garnet	
	Perovskite		Perovskite	
		Sodalite	Sodalite	
	Apatite	Apatite	Apatite	Apatite
	Magnetite		Magnetite	Magnetite
Groundmass		Sanidine	Sanidine	Sanidine
	Nepheline	Nepheline	Nepheline	Nepheline
	Clinopyroxene	Clinopyroxene	Clinopyroxene	Clinopyroxene
		Potassicarfvedsonite		
		Sodalite	Sodalite	Sodalite
			Aenigmatite	
	Götzenite	Götzenite	Götzenite	
	Barytolamprophyllite	Barytolamprophyllite		
		"Delhayelite"		
	Magnetite	Magnetite	Magnetite	Magnetite
	Pyrrhotite	Pyrrhotite	Pyrrhotite	Pyrrhotite
		Galena		
				Ilmenite
Inclusions in phenocrysts[a]	Wollastonite	K–Cl–Fe–sulfide	Chalcopyrite	Götzenite
	Sodalite		Cuspidine	
Samples	SAD 6, 10, 16d	SAD 11	SAD 1, 2, 11b, 14, 16, 16a, 16b, 16c,	SAD 4, 5, 7, 9, AF 721

Clinopyroxene: diopside, hedenbergite and aegirine-augite; garnet: andradite, schorlomite and morimotoite. "Delhayelite"—a delhayelite-group mineral intermediate between delhayelite and hydrodelhayelite. K–Cl–Fe–sulfide—chlorbartonite or Fe-dominant djerfisherite.

[a] Phenocryst minerals contain numerous inclusions of minerals which also occur as microphenocrysts and in the groundmass, only minerals which do not occur somewhere else are listed here.

Titanite is a typical minor mineral in all nephelinites and in phonolite. It occurs as euhedral and subhedral pheno- and microphenocrysts, some crystals are twinned and zoned (Fig. 7a). Corroded relics of perovskite were observed in some titanite crystals and the mineral itself can be replaced by schorlomite, morimotoite, aenigmatite or götzenite (Fig. 7b, c). The titanite has a variable minor and trace element composition—it contains between 1.2 and 2.5 wt.% Fe_2O_3, 0.1–2.3 wt.% Al_2O_3, 0.2–1.3 wt.% Nb_2O_5 (2.2 wt.% in one analysis), 0–1.0 wt.% $LREE_2O_3$ (2.3 wt.% in one analysis), 0.1–0.7 wt.% ZrO_2 and 0.1–0.4 wt.% Na_2O (Table 2, Supplementary Table 10). Fluorine was not determined during microprobe analyses of pheno-and microphenocrysts. A single analysis of titanite occurring as an inclusion in a nepheline phenocryst showed a fluorine content of 0.6 wt.%.

Perovskite occurs in nephelinites I and III, where it forms subhedral to anhedral phenocrysts (rarely) and microphenocrysts, and occurs as corroded relics in titanite phenocrysts (Fig. 7b). BSE images show complex internal zoning of the mineral owing to crystal growth, partial dissolution and late-stage alteration around inclusions and along cracks and crystal boundaries (Fig. 7d). Light rare earth elements (La to Sm) are typical minor components in the perovskite, and the content of $LREE_2O_3$ ranges from 0.8 to 4.9 wt.%. The mineral also contains Nb (0.8–1.6 wt.% Nb_2O_5), Fe (0.8–1.2 wt.% Fe_3O_2), Na (0.5–1.3 wt.% Na_2O) and traces of Th (≤0.4 wt.% ThO_2) (Table 2, Supplementary Table 11). The lowest concentrations of these elements are observed in "rims" of zoned relics of perovskite in titanite (Fig. 7b), while late-stage alteration of the mineral resulted in a reduction of the element content compared to the unaltered crystal zones (Supplementary Table 11). The chondrite-normalized REE distribution in perovskite shows two distinct groups on the basis of La/Ce_{CN} and La/Nd_{CN} ratios—perovskite microphenocrysts have lower element ratios (La/Ce_{CN} = 0.6–0.9 and La/Nd_{CN} = 1.2–1.8) compared to those of relics of perovskite in titanite ((La/Ce_{CN} = 1.1–2.5 and La/Nd_{CN} = 1.9–5.8).

Feldspar was reported to be a rare mineral in the Sadiman rocks (Mollel et al., 2011), but was found to be a common minor and accessory mineral in nephelinites III and IV; rarely it occurs in nephelinite II and no sanidine was found in nephelinites I. The mineral occurs as microphenocrysts and as micro-lathes in the nephelinite groundmass (Fig. 8a). Generally, its composition varies between $Or_{83}Ab_{12}others_5$ and $Or_{46}Ab_{41}others_{13}$ (Fig. 8c). Chemical zonation is related to variations in Ba and Sr contents. Barium concentrations in the crystal cores reach up to 4.6 wt.% BaO, and decrease towards the rim to 0.2 wt.%. SrO concentrations are below detection limit (<0.02 wt.%) at the rims and reach 0.6 wt.% in the cores (Table 2, Supplementary Table 12).

In the phonolite, sanidine occurs as both pheno- and microphenocrysts. The mineral shows a well-developed zonation in BSE images, typically with a bright core (high mean Z) and dark rims (low mean Z) in the nephelinites and rhythmic zonation (alternation of bright and dark zones) in the phonolites (Fig. 8). Sanidine from the phonolite has a high content of Na with some analyses plotting within the anorthoclase field (Fig. 11). The composition varies between $Or_{45}Ab_{51}others_4$ (crystal rim) and $Or_{29}Ab_{61}others_{10}$ (crystal core). BaO reaches 3.2 wt.% and SrO is up to 1.0 wt.% (Table 2, Supplementary Table 12).

Sodalite is a common mineral in nephelinite III where it occurs as euhedral microphenocrysts and subhedral grains in the groundmass (Figs. 7c, 8a). Few crystals were observed in nephelinites II and IV,

Table 2
Selected individual electron microprobe analyses of minerals from Sadiman rocks.

Rock	Neph I	Neph II	Neph III	Phonolite	Neph IV	Neph III		Neph IV	Neph II	Neph III	Neph I	Neph III	Neph II	Neph I	Neph III	Neph III		Neph III	Neph III	Neph III	Phonolite
Sample	SAD 10	SAD 11	SAD 16	SAD 16a	SAD 9	SAD 1		SAD 9	SAD 11	SAD 16a	SAD 10	SAD 2	SAD 11	SAD 16d	SAD 16a	SAD 1		SAD 1	SAD 2	SAD 16	SAD 16a
Mineral	Nepheline				Clinopyroxene				Garnet			Titanite		Perovskite				Feldspar			
SiO_2	42.03	43.04	44.82	46.46	48.44	47.88	49.01	47.56	31.01	29.78	27.48	30.09	30.18					61.76	64.84	64.38	65.69
TiO_2					0.59	1.66	0.57	1.02	11.45	13.88	17.31	37.45	35.59	56.17	55.35	56.79	57.74				
Al_2O_3	32.71	33.63	32.03	31.11	1.21	3.63	1.22	0.85	2.15	0.74	1.90	1.08	1.10	0.09	0.10	0.09	0.07	18.62	18.08	18.98	19.50
Fe_2O_3[a]	1.46	1.10	0.86	1.31	10.84	4.89	6.26	11.99	18.05	18.43	15.17	1.33	2.12	0.94	0.98	0.97	0.79	1.17	1.05	0.46	0.45
FeO[a]					10.51	6.70	14.13	12.86	4.24	4.43	4.66										
MnO					0.53	0.24	0.54	0.57	0.36	0.32	0.31		0.05			0.04	0.04				
MgO					5.29	10.39	5.62	3.05	0.43	0.59	0.99	0.03	0.04			0.02	0.03				
CaO	0.11	0.34	0.02	0.34	19.20	22.93	21.28	18.12	32.54	32.15	32.14	28.04	27.68	38.60	37.35	38.52	39.47	0.03		0.04	0.28
Na_2O	15.51	16.53	17.45	17.50	2.88	0.84	1.54	3.38	0.22	0.33	0.22	0.09	0.10	0.64	0.88	0.68	0.54	1.62	2.48	4.54	6.74
K_2O	7.86	6.21	4.28	2.57														13.46	13.28	9.58	6.53
SrO												0.12	0.18					0.25	0.05	0.28	0.51
BaO																		3.25	0.14	1.60	0.81
Sc_2O_3															0.03		0.03				
V_2O_3									0.26	0.16	0.16				0.04	0.04	0.06				
ZrO_2					0.03	0.04	0.03	0.04	0.33	0.23	0.36	0.16	0.28								
Nb_2O_5												0.42	1.29	1.01	1.02	0.71	0.81				
ThO_2														0.12	0.24	0.09					
La_2O_3												0.10		0.41	0.65	0.66	0.42				
Ce_2O_3												0.18	0.34	1.44	2.25	1.15	0.45				
Pr_2O_3														0.19	0.24	0.12					
Nd_2O_3												0.12	0.16	0.59	0.88	0.40	0.14				
Sm_2O_3												0.07		0.13	0.14	0.05					
Total	99.67	100.86	99.46	99.29	99.53	99.20	100.20	99.45	101.03	101.04	100.70	99.28	99.11	100.32	100.16	100.31	100.59	100.16	99.92	99.86	100.50
Structural formulae																					
Si	4.109	4.120	4.297	4.415	1.904	1.831	1.923	1.900	2.587	2.504	2.315	0.996	1.005					2.917	2.985	2.957	2.953
Ti					0.017	0.048	0.017	0.031	0.719	0.878	1.097	0.932	0.891	0.972	0.968	0.979	0.984				
Al	3.768	3.794	3.619	3.484	0.056	0.164	0.056	0.040	0.212	0.073	0.189	0.042	0.043	0.002	0.003	0.002	0.002	1.037	0.981	1.027	1.033
Fe^{3+}	0.107	0.079	0.062	0.094	0.321	0.140	0.184	0.360	1.133	1.166	0.962	0.033	0.053	0.016	0.017	0.017	0.013	0.042	0.036	0.016	0.015
Fe^{2+}					0.346	0.214	0.463	0.430	0.296	0.312	0.328										
Mn					0.018	0.008	0.018	0.019	0.026	0.023	0.022		0.001			0.001	0.001				
Mg					0.310	0.592	0.328	0.182	0.053	0.074	0.124	0.001	0.002			0.001	0.001				
Ca	0.011	0.035	0.002	0.035	0.809	0.940	0.894	0.776	2.909	2.897	2.902	0.994	0.987	0.952	0.930	0.946	0.959	0.001	0.000	0.002	0.014
Na	2.939	3.068	3.243	3.224	0.219	0.062	0.117	0.262	0.035	0.054	0.036	0.006	0.006	0.029	0.040	0.030	0.024	0.149	0.221	0.404	0.587
K	0.980	0.758	0.523	0.311														0.811	0.780	0.561	0.374
Sr												0.002	0.003					0.007	0.001	0.008	0.013
Ba																		0.060	0.003	0.029	0.014
Sc															0.001		0.001				
V									0.017	0.011	0.011				0.001	0.001	0.001				
Zr					0.001	0.001		0.001	0.014	0.009	0.015	0.003	0.005								
Nb												0.006	0.019	0.011	0.011	0.007	0.008				
Th														0.001	0.001						
La												0.001		0.004	0.006	0.006	0.003				
Ce												0.002	0.004	0.012	0.019	0.010	0.004				
Pr														0.002	0.002	0.001					
Nd												0.001	0.002	0.005	0.007	0.003	0.001				
Sm												0.001		0.001	0.001						
Total	11.913	11.856	11.746	11.563	4.000	4.000	4.000	4.000	8.000	8.000	8.000	3.022	3.023	2.005	2.006	2.005	2.002	5.024	5.007	5.004	5.004

The samples are organized (1) in order of mineral description in the manuscript and (2) to show range in major and minor elements. Neph I—nephelinite I, Neph II—nephelinite II, Neph III—nephelinite III, Neph IV—nephelinite IV.

[a] For nepheline, titanite, perovskite and feldspar all Fe as Fe_2O_3, for clinopyroxene and garnet Fe_2O_3 and FeO calculated from charge balance. Mineral formulae were calculated for O = 16 (nepheline), 4 cations and O = 6 (clinopyroxene), 8 cations and O = 12 (garnet), O = 4 (titanite), O = 3 (perovskite) and O = 8 (feldspar).

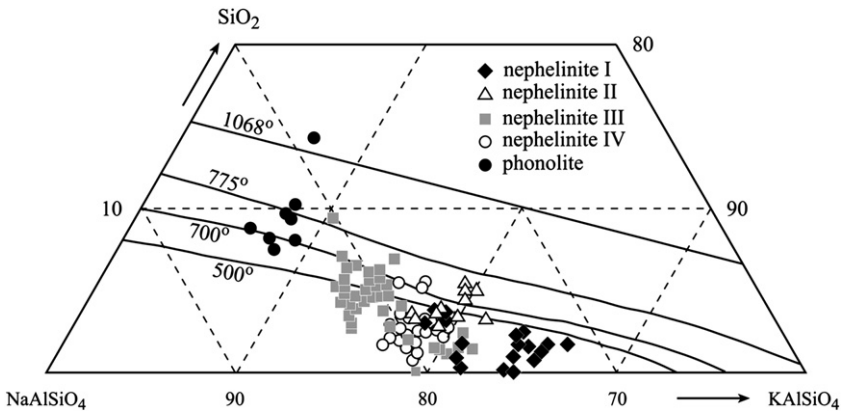

Fig. 3. Nepheline compositions (wt.%) from the nephelinites and phonolite. The isotherms are from Hamilton (1961).

and it occurs rarely as solid inclusions in garnet phenocrysts in the nephelinite I. The chemical composition of the sodalite is close to its ideal formula with only minor amounts of Fe (0.7–1.4 wt.% Fe_2O_3), S (<0.3 wt.% SO_3) and K (<0.2 wt.% K_2O) detected by EDS analysis (Supplementary Table 13).

Aenigmatite was observed in nephelinite III only, where it occurs in the groundmass and as replacement rims on titanite pheno- and microphenocrysts (Fig. 7c). Formulae calculated on the basis of charge balance suggest the presence of significant amounts of Fe^{3+} (4.8–6.0 wt.% Fe_2O_3) (Supplementary Table 14). The mineral is a sodium-rich variety, with 2.16–2.31 apfu of Na. We suggest that part of the Na in the studied aenigmatite can be accommodated within the Fe^{2+} site as observed for synthetic aenigmatite-type compounds (Redhammer et al., 2008).

Götzenite is occasionally present in all nephelinite types. The mineral occurs as small anhedral grains in the groundmass and inclusions

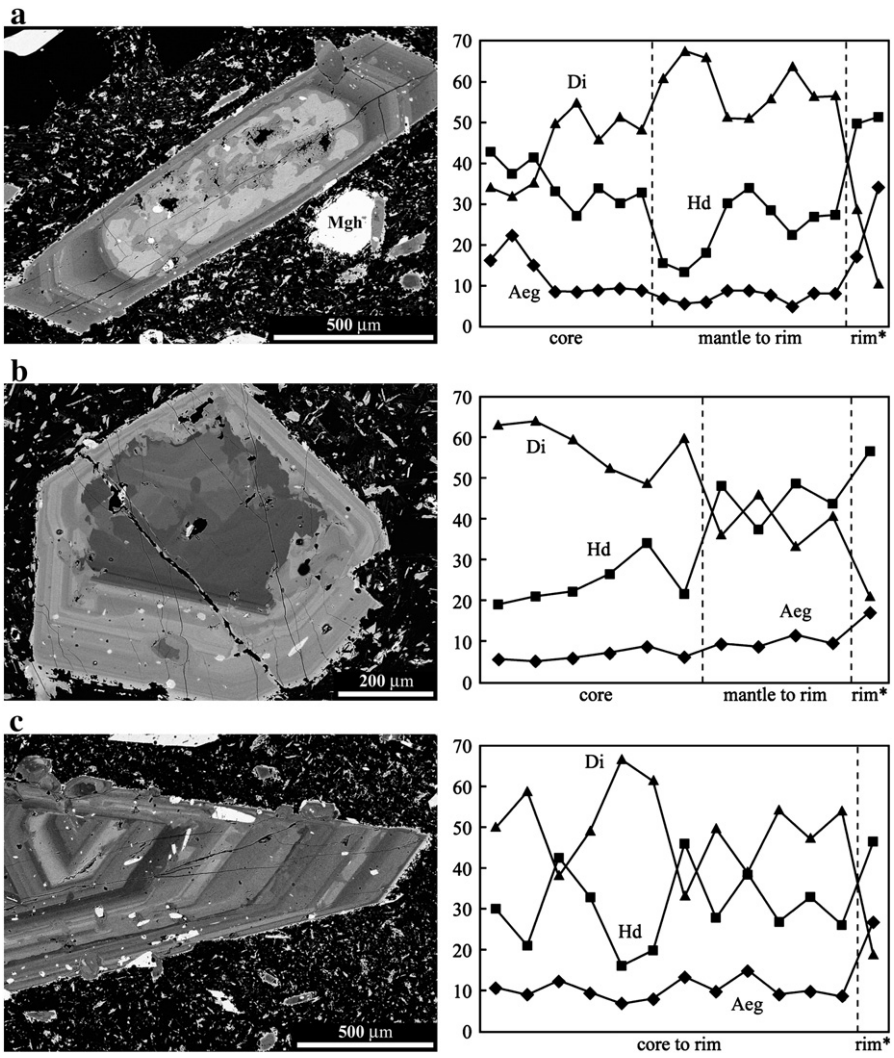

Fig. 4. BSE images of various crystal types of clinopyroxene and zoning profiles showing variations in their end-member compositions (mol.%). (a) Nephelinite IV, sample SAD 9, (b) nephelinite III, sample SAD 1, (c) nephelinite IV, sample SAD 9. Mgh—magnetite, Di—diopside, Hd—hedenbergite, Aeg—aegirine. rim*—bright fine rim surrounding phenocrysts.

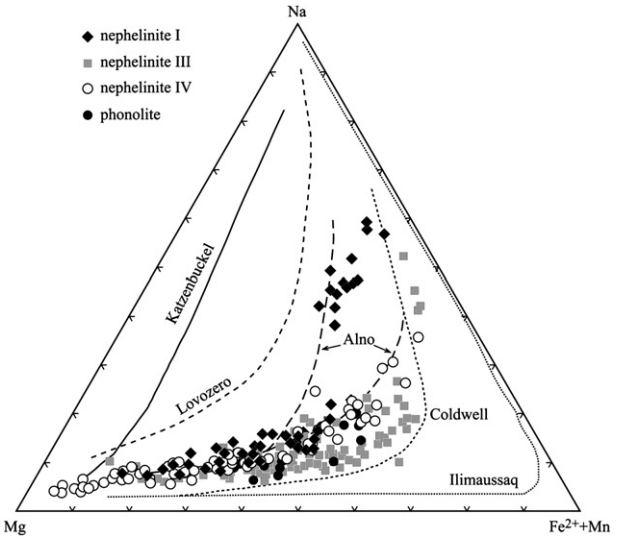

Fig. 5. Compositional variations of the clinopyroxenes in the system Na–Mg–Fe^{2+} + Mn (at.%). Clinopyroxene trends are from Katzenbuckel (Mann et al., 2006), Lovozero (Korobeinikov and Laajoki, 1994), Alnö (Vuorinen et al., 2005), Coldwell (Mitchell and Platt, 1982) and Ilímaussaq (Larsen, 1976; Marks and Markl, 2001; Markl et al., 2001).

within clinopyroxene phenocrysts, and it also forms reaction rims and cross-cutting veinlets in schorlomite and titanite (Fig. 6a). The mineral compositions obtained by SEM-EDX analysis are close to the ideal formula of götzenite, $Na_2Ca_5Ti(Si_2O_7)_2F_4$.

Magnetite is an accessory mineral in nephelinites and phonolite and occurs as subhedral and partly corroded grains in the groundmass (Fig. 4a) and as inclusions in pyroxene and nepheline. The grains are commonly corroded and replaced by Si-rich iron hydroxide. One sample of nephelinite IV contains a few crystals of subhedral magnetite with ilmenite exsolutions while another sample contains apparent "ore droplets" consisting of magnetite, pyrrhotite, and ilmenite.

Magnetite is a titanium-rich variety with the TiO_2 content between 8.8 (in nephelinite I) and 18.9 wt.% TiO_2 (in nephelinites III and IV) (Supplementary Table 15). The mineral also contains minor Mn (0.5–2.2 wt.% MnO), Al (0–1.0 wt.% Al_2O_3), Mg (up to 0.5 wt.% MgO) and traces of Zn (up to 0.3 wt.% ZnO), Nb and Zr (<0.1 wt.% oxides). Minor elements (Mn, Al and Mg) show that the composition of magnetite is heterogeneous and that a single sample can contain grains with quite different element concentrations. We interpret this to indicate a xenocrystic origin for at least some of the crystals.

Pyrrhotite occurs as rounded or oval inclusions (blebs) in phenocryst minerals (nepheline, pyroxene and titanite). Phenocryst-hosted blebs rarely show a chalcopyrite rim around pyrrhotite. It is also present within the groundmass and is associated with magnetite and ilmenite in "ore droplets". The mineral contains Cu (up to 0.8 wt.%) and Mn (up to 0.2 wt.%); the (Fe + Cu + Mn)/S ratio ranges from 0.89 to 0.93 (Supplementary Table 16).

Chlorine-bearing potassium sulfide in association with pyrrhotite was found in one bleb (20 μm) within a nepheline phenocryst. The chemistry of this sulfide (EDS, normalized to 100%, average from five analyses, wt.%: K = 9.3, Fe = 52.5, Cu = 1.5, S = 35.3; Cl = 1.4) shows that it may be both chlorbartonite and Fe-dominant djerfisherite.

Ilmenite was found in one sample of nephelinite IV as an intergrowth with magnetite. It also occurs as exsolution lamellae within magnetite in nephelinite IV. Calculated mineral formulae suggest the presence of essential amounts of Fe^{3+} in the ilmenite (Fe_2O_3calc = 7.0–8.5 wt.%), with minor Mn (3.3–3.4 wt.% MnO), Mg (0.3–0.4 wt.% MgO), V (0.2–0.3 wt.% V_2O_3) and Nb (0.1–0.2 wt.% Nb_2O_5) (Supplementary Table 17).

A delhayelite-group mineral was found as a principal groundmass phase in sanidine-poor nephelinite II. The chemical composition (WDS, averaged from ten analyses, wt.%: SiO_2 = 54.99, TiO_2 = 0.03, Al_2O_3 = 6.42, Fe_2O_3 = 1.25, MnO = 0.04, MgO = 0.04, CaO = 16.81, BaO = 0.15, SrO = 0.70, Na_2O = 6.36, K_2O = 6.53, F = 2.60, Cl = 2.34, S = 0.01, O = $(F,Cl)_2$ = 1.63, total = 96.64) indicates a formula close to $KNa_2Ca_2[AlSi_7O_{17}(OH)_2]FCl_{0.5}(OH)_{0.5}$. This mineral (potentially, a new mineral species) is intermediate between delhayelite $K_4Na_2Ca_2[AlSi_7O_{19}]F_2Cl$ and hydrodelhayelite $KCa_2[AlSi_7O_{17}(OH)_2]\cdot(6-x)H_2O$ (Pekov et al., 2009). It is homogeneous in composition and seems to be a primary phase within the groundmass and is closely associated with aegirine and potassicarfvedsonite. A delhayelite-like mineral with the same composition was previously described as a groundmass phase in peralkaline phonolite from Saghro, SE Morocco (Berger et al., 2009).

5. Bulk geochemistry

The bulk rock compositions (Table 3) show that the studied nephelinites are low-magnesium rocks (atomic Mg/(Mg + Fe) = 0.17–0.26) with an alkalinity index [molar (Na + K)/Al] ranging between 0.88 and 1.21. On a volatile-free basis these rocks contain 46.3–52.6 wt.% SiO_2 and 10.5–15.9 wt.% $Na_2O + K_2O$. In the total alkali–silica (TAS) diagram, data form a broad field with the majority of points plotting in the foidite and phonolite fields (Fig. 9) (this study and Dawson, 2008, Paslick et al., 1995 and Mollel et al., 2011). There is an increase in silica and alkali element concentrations from nephelinite I to nephelinites III and IV.

The trace element composition is characterized by 1530–2460 ppm Sr, 1475–2770 ppm Ba, 144–230 ppm Nb, 341–483 ppm Zr and 350–637 ppm REEs (Table 3). The element pattern is similar to that published by Mollel et al. (2011) with the exception of his sample 04-NT-3 (described as a phonolite from a Sadiman lahar deposit in the Noiti area, about 20–25 km south-west of Sadiman) which shows low concentrations of U, Zr and Hf. All studied nephelinite samples show negative P

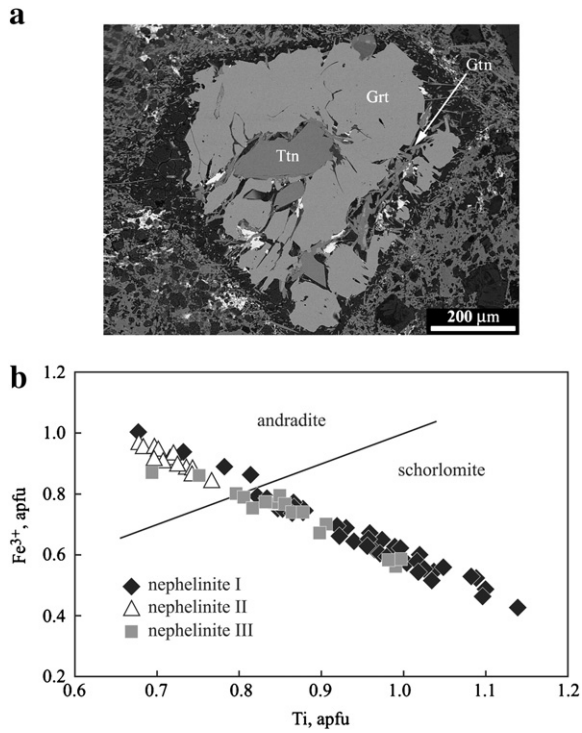

Fig. 6. Garnet in nephelinites—(a) BSE image of garnet microphenocryst (Grt) with relics of titanite (Ttn), a replacement rim of a Ca–Na–K aluminosilicate (black) and a veinlet of götzenite (Gtn), nephelinite I, sample SAD 10; (b) compositional variations of garnet on its *Y* site (Ti vs Fe^{3+}, apfu); line with slope 1:1 separates fields of andradite and schorlomite.

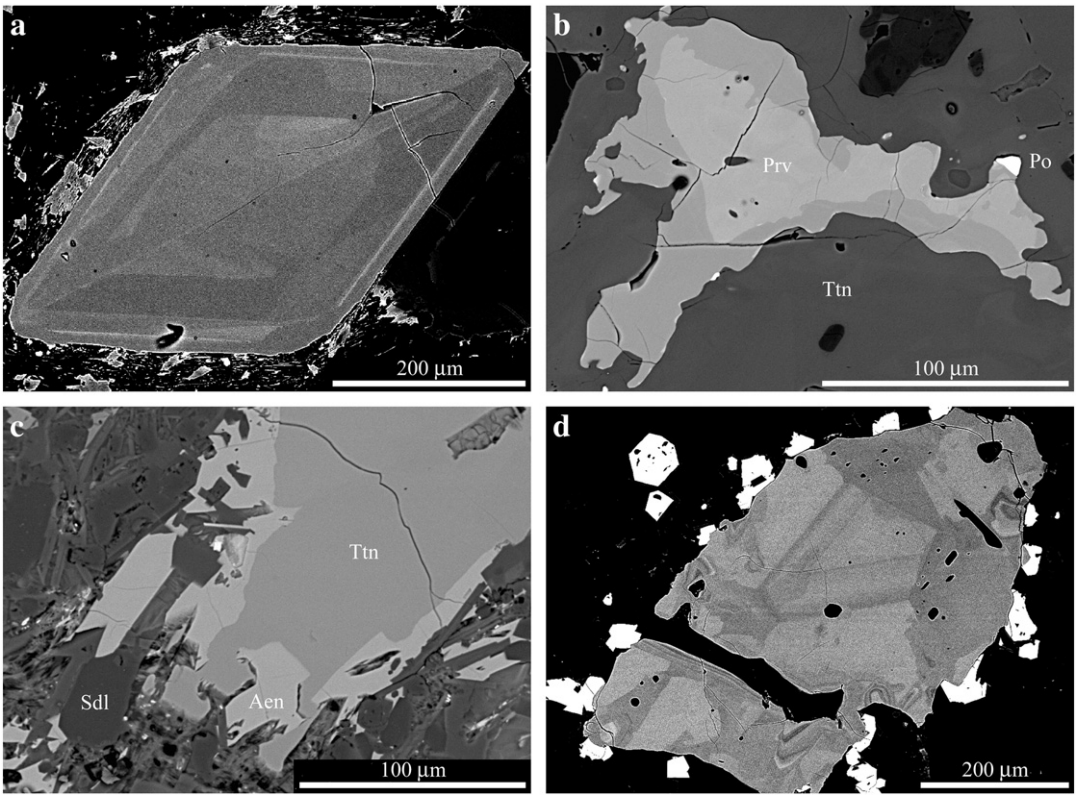

Fig. 7. BSE images of titanite and perovskite from nephelinites: (a) twinned and zoned titanite microphenocryst, nephelinite II, sample SAD 11; (b) perovskite relic (Prv) in titanite (Ttn), Po—pyrrhotite, nephelinite III, sample SAD 1; (c) titanite (Ttn) with aenigmatite (Aen) reaction rim, Sdl—sodalite, nephelinite III, sample SAD 2; (d) anhedral perovskite microphenocryst (gray) with overgrown magnetite (white), nephelinite I, sample SAD 16d.

and Ti anomalies and a positive Pb anomaly. Chondrite-normalized rare earth elements show similar parallel patterns, displaying an enrichment in light REE with a $(La/Yb)_{CN}$ ratio of 32.5–39.2 (Fig. 10).

6. Melt inclusions

Primary silicate melt inclusions were observed in phenocrysts and microphenocrysts of the Sadiman nephelinites—they occur in nepheline, titanite, diopside–hedenbergite, apatite, wollastonite and sanidine and are most abundant in nepheline. Primary silicate melt inclusions, together with crystal inclusions (diopside, titanite, apatite), commonly outline the growth zones in host nepheline phenocrysts. Primary fluid and sulfide inclusions are rare; trails of secondary melt inclusions occur scarcely.

Melt inclusions (10–100 μm) in nepheline are highly variable in phase composition (Fig. 11). Some nephelinite samples contain abundant glassy

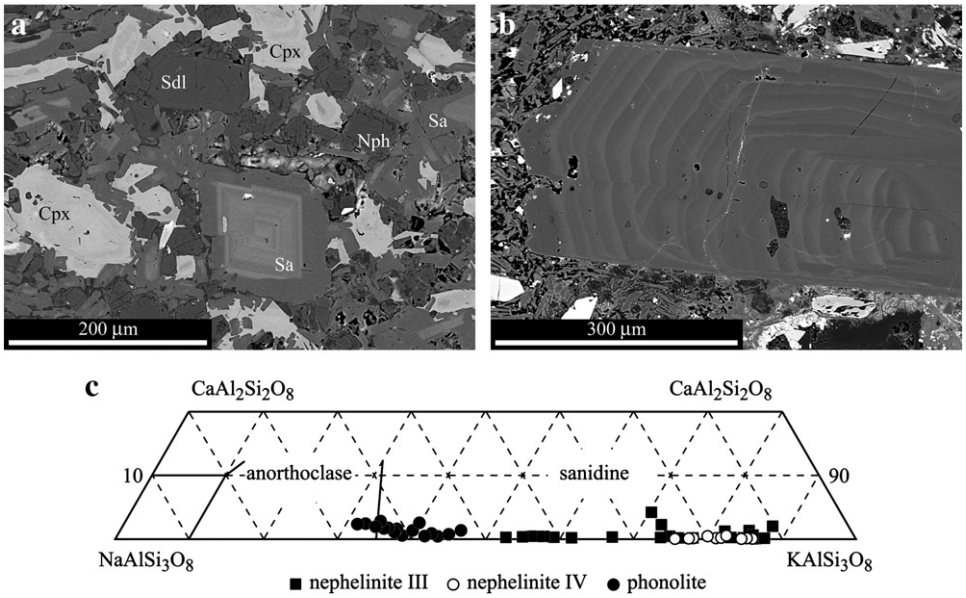

Fig. 8. BSE images of (a) sanidine (Sa) in nephelinite III groundmass, Cpx—diopside–hedenbergite, Sdl—sodalite, Nph—nepheline, sample SAD 16, (b) zoned sanidine–anorthoclase phenocryst in phonolite, sample SAD 16a and (c) compositional variations of feldspar in the system $CaAl_2Si_2O_8$–$NaAlSi_3O_8$–$KalSi_3O_8$ (mol.%).

Table 3
Major and trace element composition of the Sadiman nephelinites.

Type	I	II	III					IV		
Sample	SAD 10	SAD 11	SAD 1	SAD 2	SAD 16	SAD 16b	SAD 16c	SAD 4	SAD 5	SAD 9
wt.%										
SiO_2	43.39	45.37	50.67	48.60	50.74	50.21	50.89	49.52	49.26	49.00
TiO_2	1.27	1.06	0.83	1.09	0.97	0.59	1.00	1.42	1.10	1.39
Al_2O_3	16.57	16.17	19.26	18.72	19.31	22.93	19.29	17.87	18.34	17.60
Fe_2O_3	10.00	9.15	7.37	8.42	7.20	5.76	7.24	8.73	8.49	8.48
MnO	0.26	0.25	0.17	0.18	0.17	0.11	0.17	0.19	0.19	0.17
MgO	1.33	0.84	0.71	1.30	0.89	0.35	0.94	1.29	1.04	1.53
CaO	10.65	9.22	3.93	5.28	4.85	2.19	4.46	6.03	4.98	6.32
Na_2O	7.02	9.34	8.52	6.83	8.40	10.69	8.17	7.68	7.55	7.11
K_2O	2.83	3.85	5.59	5.18	4.40	4.84	4.51	4.43	5.51	4.62
P_2O_5	0.35	0.30	0.12	0.17	0.17	0.08	0.17	0.29	0.18	0.29
LOI	5.75	3.53	1.59	3.08	3.67	1.51	1.94	1.77	3.20	3.11
Total	99.42	99.07	98.76	98.85	100.77	99.25	98.79	99.21	99.83	99.62
Cl ppm	220	3810	2890	2150	1270	2960	2680	680	2660	1260
F	1740	2540	650	1070	450	320	400	300	1560	460
S	60	920	330	40	40		40	20	250	350
(K + Na)/Al	0.88	1.21	1.04	0.90	0.96	1.00	0.95	0.98	1.00	0.95
Mg#	23.0	17.0	17.8	25.7	21.8	12.1	22.6	24.9	21.6	28.9
ppm										
Li	34.6	47.4	11.6	9.31	29.2	7.11	9.39	35.6	6.71	26.6
Be	8.20	10.8	8.17	7.35	7.86	9.09	8.23	7.24	8.33	7.24
Sc	1.63	1.48	1.71	2.02	1.80	0.73	1.87	2.93	2.11	4.53
V	138	153	72.9	108	71.1	25.8	75.9	116	106	123
Co	17.0	11.8	11.0	13.7	10.9	6.31	11.5	16.4	14.5	17.5
Ni	2.92	3.36	1.91	2.41	2.02	0.89	2.05	3.78	2.35	5.45
Cu	74.2	36.9	47.7	61.9	48.4	25.2	36.7	74.4	60.3	71.8
Zn	162	193	162	157	150	162	159	153	171	149
Rb	91.7	85.8	188	257	118	134	119	107	180	158
Sr*	2448	2460	1730	1950	1750	1530	2060	1750	1790	1750
Y	33.3	55.8	29.2	29.5	28.1	34.4	30.1	29.7	31.1	27.4
Zr	347	483	377	341	359	415	380	366	366	344
Nb	206	230	146	150	156	181	162	165	161	144
Mo	1.72	5.27	3.12	1.31	1.83	0.95	2.65	1.31	1.83	1.18
Cd	0.40	0.61	0.39	0.42	0.35	0.35	0.36	0.41	0.38	0.31
Sb	0.356	0.512	0.366	0.364	0.208	0.290	0.320	0.250	0.338	0.500
Cs	0.58	0.69	2.34	1.73	1.30	1.45	1.22	1.57	0.92	1.62
Ba*	1853	2041	2014	1873	1475	1917	1545	1782	2049	2770
Hf	7.07	9.33	8.20	7.69	7.37	7.70	7.47	7.94	7.88	7.37
Ta	6.60	5.01	3.69	4.38	5.35	4.93	5.26	6.70	4.59	5.44
W	1.44	2.50	1.77	0.84	1.70	0.77	1.04	3.29	0.85	1.28
Tl	0.184	0.417	0.836	0.414	0.211	0.402	0.291	0.200	0.340	0.181
Pb	22.6	33.7	24.6	22.0	23.4	26.1	24.9	23.3	24.1	22.5
Th	15.2	29.1	24.7	18.7	24.2	25.5	24.1	21.8	20.5	20.8
U	4.21	7.30	5.52	4.93	5.27	3.49	5.21	3.46	4.76	4.57
ppm										
La	138	186	109	104	108	122	109	112	109	97.3
Ce	213	286	167	161	171	196	173	183	169	160
Pr	19.8	26.8	14.5	14.7	15.6	17.0	15.9	17.7	15.4	14.8
Nd	63.8	84.5	46.1	47.3	49.8	53.7	51.7	58.9	49.9	49.8
Sm	9.73	13.6	7.14	7.53	7.56	8.03	7.85	9.21	7.89	7.86
Eu	2.84	4.01	2.08	2.19	2.18	2.35	2.31	2.58	2.31	2.24
Gd	8.23	12.1	6.11	6.51	6.12	6.72	6.53	7.38	6.84	6.54
Tb	1.08	1.69	0.868	0.897	0.849	0.948	0.885	0.988	0.947	0.874
Dy	5.87	9.60	5.05	5.10	4.82	5.53	5.11	5.48	5.40	4.83
Ho	1.10	1.84	0.987	0.980	0.924	1.10	0.990	1.02	1.04	0.919
Er	2.99	5.04	2.79	2.68	2.59	3.11	2.76	2.77	2.86	2.51
Tm	0.397	0.675	0.379	0.358	0.351	0.423	0.378	0.366	0.386	0.335
Yb	2.52	4.10	2.36	2.27	2.20	2.66	2.38	2.30	2.40	2.11
Lu	0.374	0.565	0.336	0.320	0.306	0.360	0.328	0.324	0.337	0.292
Total REE	470	637	365	356	372	419	379	404	374	350

Elements given as oxides and Cl, F and S are determined by XRF. Other elements are determined by ICP-MS except elements marked with "*" that are determined using ICP-AES.

(greenish glass + gas; glass + gas + daughter fluorite) or partly crystallized inclusions (glass + gas + daughter crystals ± trapped crystals), whereas other samples contain only party crystallized or translucent completely crystallized inclusions (daughter crystals + gas ± glass). Aegirine, potassicarfvedsonite, sanidine and fluorcanasite are principal daughter phases in the crystallized inclusions. Gas bubbles in partly crystallized inclusions commonly contain some amount of unidentified salt phases. No melt inclusions with clear silicate–carbonate liquid immiscibility as in the Oldoinyo Lengai nephelines (Mitchell, 2009; Sharygin et al., 2012-this issue) were observed at Sadiman. It

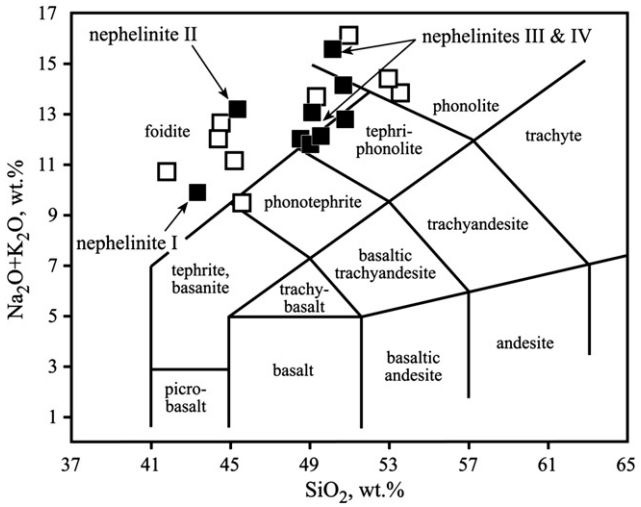

Fig. 9. TAS-diagram for Sadiman lavas. Filled square—data from this study, open square—published data (James, 1966; Mollel et al., 2011; Paslick et al., 1995).

should be noted that fluorite is a common daughter phase in all of the nepheline-hosted inclusions.

Melt inclusions in titanite, diopside–hedenbergite, and wollastonite commonly have the following phase composition: glass + gas ± daughter crystals ± trapped crystals. Apatite-hosted inclusions mainly consist of daughter minerals (salt(s)?) and gas bubble. Rare inclusions in sanidine are finely devitrified.

About 50 heating experiments were conducted on the mineral-hosted inclusions in two nephelinite samples, and data on homogenization temperatures are given in Table 4. Nepheline-hosted inclusions show various phase compositions and phase behavior during heating. These are susceptible however, to leakage during experiments, especially at temperatures higher than 800 °C. The same problems were described by Bazarova et al. (1975) for nepheline-hosted inclusions in nephelinites. They explained that inclusion leakage results from the structural inversion in nepheline at about 850 °C. Nevertheless, we successfully homogenized some individual inclusions, while the majority of inclusions demonstrated leakage in the 800–900 °C range. During heating from 20–25 °C to 850 °C we observed the following phase transformations: transition of silicate glass into silicate liquid (560–600 °C); melting of daughter fluorite in the CaF_2 liquid (600–630 °C); melting of daughter silicate phases (620–710 °C); amalgamation of the CaF_2 bleb and gas bubble (630–680 °C); decrease of the gas bubble's size and of the CaF_2 bleb or unified CaF_2-gas bubble (750–850 °C). Heating experiments showed the existence of silicate-CaF_2 liquid immiscibility during cooling of the Sadiman nephelinite magma.

The homogenization temperature for inclusions from the outer and middle zones of the nepheline phenocrysts is 860–930 °C, and for inclusions from the central zones, it is 970–1100 °C. These results agree closely with homogenization temperatures given for inclusions in nepheline by Bazarova et al. (1975) for nephelinite sample AF-721 from Sadiman (Table 4). Much higher temperatures (1180–1300 °C) have been reported for melt inclusions in nepheline by Naumov et al. (1972).

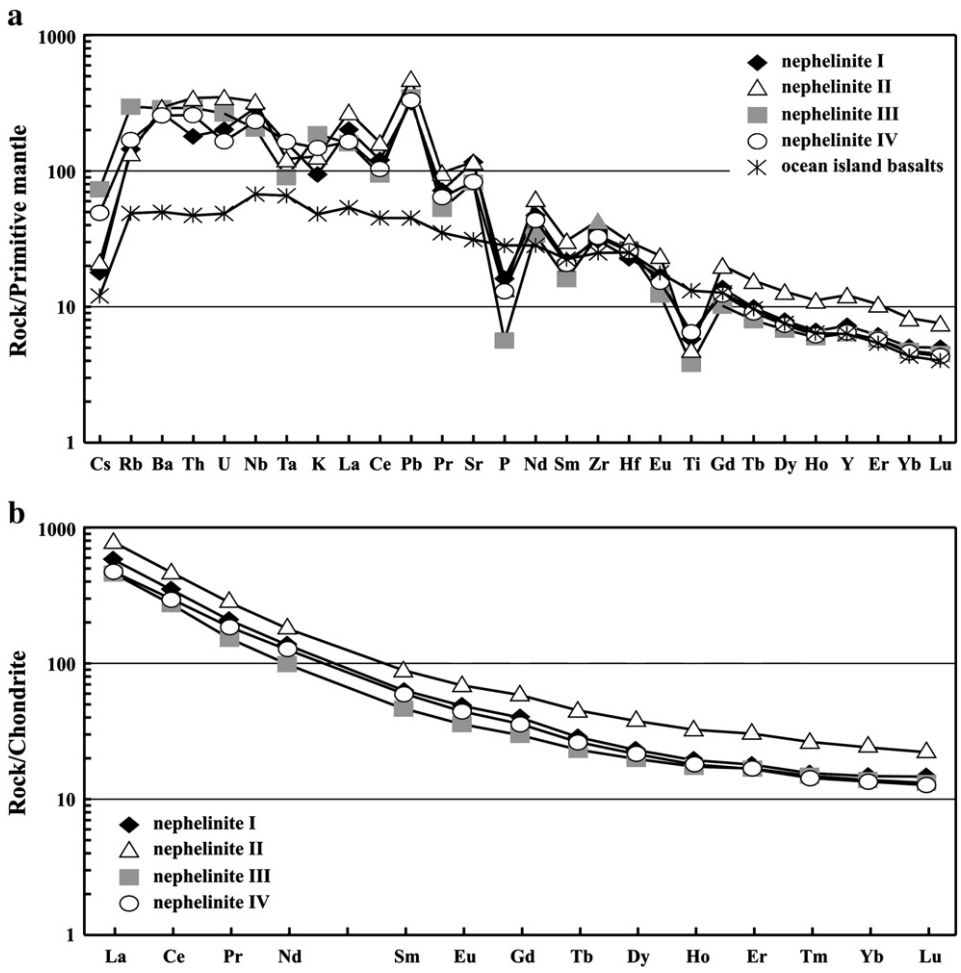

Fig. 10. Primitive mantle- and chondrite-normalized plots for the Sadiman nephelinites. Data for ocean island basalts, normalizing values for primary mantle and chondrite are from Sun and McDonough (1989).

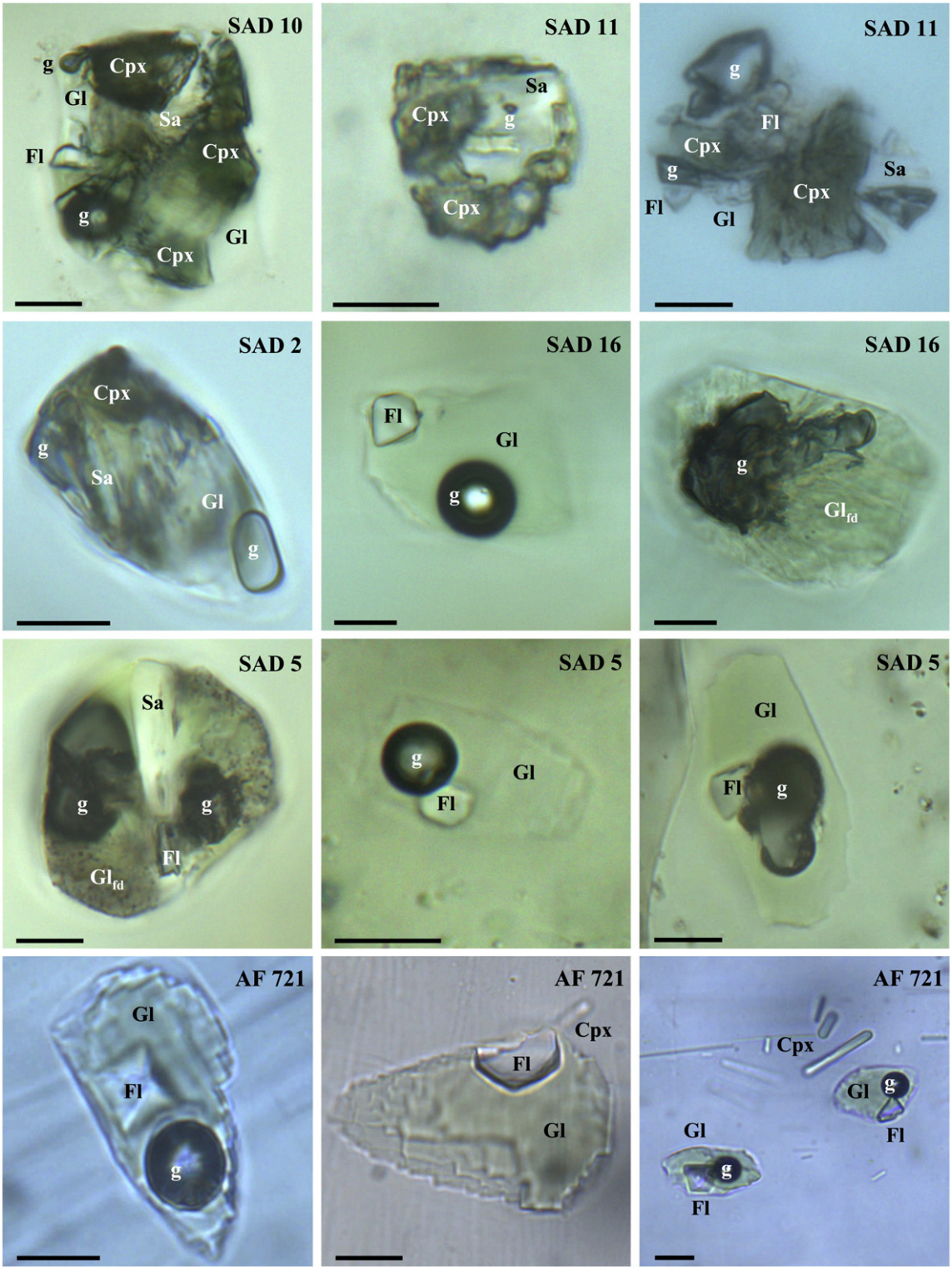

Fig. 11. Silicate melt inclusions with different phase compositions in nepheline phenocrysts. Scale bar—10 μm. Symbols: Gl—glass; Gl_{fd}—finely devitrified glass; Cpx—clinopyroxene; Sa—sanidine(?); Fl—fluorite; g—gas bubble (sometimes may contains salt phases).

Chemical compositions of silicate glass from unheated glass-rich nepheline-hosted inclusions for samples SAD 11, SAD 16 and AF-721 are given in Table 5. The greenish glass is silica-saturated with SiO_2 = 55.3–58.1 wt.%, rich in Fe (FeO_{total} = 8.6–14.0 wt.%) and Na (Na_2O = 6.4–15.3 wt.%), and contains volatile components (F + Cl + SO_3 = 2.4–3.6 wt.%). The peralkalinity index of the glass is 3.4–8.9. All glasses are characterized by low totals (89–97 wt.%) suggesting the presence of other components (H_2O, CO_2, or both).

7. Discussion

7.1. Evaluation of rock types composing Sadiman

Despite the limited number of outcrops at Sadiman, the available data suggest a multiphase evolution of the volcano with punctuated effusive (lavas) and explosive (ashes—now tuffs) eruptions. Published and new data presented in this work show that nephelinite is

Table 4
Homogenization temperatures of mineral-hosted inclusions in the Sadiman nephelinites.

Sample	Mineral	T_{hom}, °C
SAD 11 (nephelinite II)	Apatite	820–970
	Wollastonite	910–1010
	Clinopyroxene	950–1000
	Nepheline	920–980
SAD 16 (nephelinite III)	Titanite	>1230
	Clinopyroxene	900–970
	Nepheline (core)	970–1100
	Nepheline (rim)	860–930
AF-721[a] (nephelinite IV)	Apatite	1200–1220
	Nepheline	880–1050

[a] Data from Bazarova et al. (1975).

the major effusive rock type at Sadiman (Dawson, 2008; Hay, 1976; Mollel, 2007; Mollel et al., 2011; Paslick et al., 1995; Zaitsev et al., 2011). New data on the petrography, mineralogy and geochemistry of the nephelinites suggest that they are represented by highly porphyritic nephelinite (type I), wollastonite nephelinite (type II) and phonolitic nephelinite (types III and IV).

Phonolites were reported to be present at the Sadiman volcano (Hay, 1976; Mollel, 2007; Mollel et al., 2011; Pickering, 1964) and one phonolite sample from Sadiman was described from a lahar deposit in the Noiti area (Mollel, 2007; Mollel et al., 2011). However, no mineralogical data were published for these phonolites and their identification was based on bulk rock geochemistry data only (Mollel, 2007; Mollel et al., 2011). Importantly, no alkali feldspar was described as a phenocrystic phase and sanidine laths were mentioned from only one sample (Mollel et al., 2011).

Melilite-bearing rocks (melilitites, melilite nephelinites) and carbonatites were mentioned to occur at Sadiman (e.g. Dawson, 2008; Woolley, 2001) and following R. Hay's publications (e.g. Hay, 1978, 1987) this volcano was considered to be the source of the melilitite–carbonatite ashes (now tuffs) deposited in the Laetoli area. Our study of Sadiman lavas and tuffs, as well as heavy mineral fractions from epiclastic rocks, did not reveal any evidence for the presence of key minerals that could be indicators of the eruption of melilititic and/or carbonatitic rocks (Wiedenmann et al., 2009, 2010; Zaitsev, 2010; Zaitsev et al., 2010). No fresh or altered/pseudomorphed åkermanite, alumoåkermanite, calcite, nyerereite, or pyrochlore were found in the studied samples. Heavy mineral fractions contain perovskite, magnetite, clinopyroxene, andradite–schorlomite, ilmenite and pyrrhotite; this mineral assemblage is similar to that in nephelinites and phonolites. A few grains of zircon, spinel–hercynite, Al_2SiO_5 (andalusite, sillimanite or kyanite) and Th-rich monazite were also found and they are considered to be xenocrystic minerals derived from basement metamorphic rocks.

Sadiman nephelinite lavas and phonolitic tuffs also contain xenoliths of nepheline–clinopyroxene plutonic rock which could be classified as ijolite (Hay, 1976; Zaitsev et al., 2011).

7.2. Mineralogical and geochemical characteristics of the nephelinites

The phenocrystic and groundmass mineral assemblages of the Sadiman nephelinites comprise nepheline + clinopyroxene + titanite ± wollastonite ± perovskite ± andradite–schorlomite ± sanidine ± sodalite (Table 1). These assemblages show that Sadiman nephelinites are quite different from primitive high-magnesium olivine ± melilite-bearing nephelinites that occur elsewhere in East Africa including northern Tanzania (e.g. Dawson et al., 1985; Keller et al., 2006; Le Bas, 1987). Although olivine has been reported from the Sadiman volcanic rocks by Mollel et al. (2011) it was not found during this study. Furthermore, the geochemical characteristics of the nephelinites (low magnesium number—17.0–28.9, and Ni (1.0–5.5 ppm; Table 3) and Cr (<10 ppm) contents) do not support the occurrence of olivine at Sadiman.

In contrast, the studied nephelinites have many similarities with highly evolved perovskite-, schorlomite- or wollastonite-bearing nephelinites known from several volcanic complexes close to Sadiman, such as Embagai, Shombole, Kerimasi and even Oldoinyo Lengai (e.g. Church, 1996; Klaudius and Keller, 2006; Mollel, 2007; Paslick et al., 1995, 1996; Peterson, 1989), and to lava flows in the western escarpment of the Lake Natron area (Neukirchen et al., 2010). These similarities are reflected in the observed range of mineral compositions, their evolutionary trends, and mineral relationships (Table 2, Supplementary Tables 6–17, Figs. 3–7). The highly evolved nature of the Sadiman nephelinites is also supported by geochemical features (Table 3).

The evolution of nephelinites from northern Tanzania has been discussed by Neukirchen et al. (2010), Paslick et al. (1995, 1996), Peterson (1989), and crystal contamination of nephelinitic melts, mixing of different magma batches, and the open system conditions of nephelinite crystallization have all been shown to be important

Table 5
Chemical composition of glass from unheated silicate melt inclusions in nepheline phenocrysts.

Sample	SAD 11	SAD 16								AF 721			
Inclusion phase composition	Gl + g	Gl + g	Gl + g	Gl + g	Gl + g	Gl + g	Gl + Fl + g	Gl + g	Gl + Fl + g	Gl + Fl + g	Gl + g	Gl + Fl + g	Gl + Fl + g
n	3	2	2	2	2	2	4	2	3	4	1	2	2
wt.%													
SiO_2	55.70	55.25	56.15	57.16	57.72	55.80	56.94	56.43	58.12	56.79	57.60	56.54	56.42
TiO_2	0.97	0.75	0.90	0.90	0.61	0.78	1.11	0.98	0.80	1.25	1.21	1.28	1.27
ZrO_2	0.18												
Al_2O_3	4.55	2.87	2.94	3.21	3.37	3.01	3.60	3.08	3.53	3.37	3.38	3.44	3.68
FeO_{total}	11.74	10.07	10.25	10.41	10.50	10.37	10.37	11.49	8.56	13.03	14.04	13.55	13.69
MnO	0.27	0.49	0.57	0.48	0.45	0.41	0.38	0.62	0.33	0.54	0.62	0.55	0.53
MgO	0.18	0.29	0.40	0.40	0.27	0.42	0.35	0.32	0.21	0.27	0.33	0.31	0.34
CaO	4.18	6.92	6.03	6.10	6.40	7.03	5.88	6.08	4.79	3.41	3.05	4.33	3.09
BaO	0.21	0.34	0.45	0.60	0.51	0.38	0.59	0.38	0.56	0.51	0.75	0.91	0.50
Na_2O	8.67	15.14	14.62	13.76	14.45	14.13	15.30	12.62	12.30	7.32	6.41	7.58	7.46
K_2O	4.96	0.51	0.52	0.56	0.56	0.51	0.60	0.56	0.85	0.68	0.78	0.71	0.70
P_2O_5	0.03	0.07	0.08	0.10	0.06	0.08	0.09	0.08	0.06	0.17	0.13	0.11	0.13
F	0.48	0.95	0.80	1.03	1.06	1.18	1.08	0.99	2.36	0.93	1.80	1.42	1.20
Cl	0.41	0.87	0.85	0.67	0.90	0.86	0.65	0.91	0.97	0.82	0.57	0.79	0.84
SO_3	0.41	0.33	0.41	0.35	0.17	0.26	0.33	0.31	0.25	0.66	0.55	0.54	0.63
$-O-(F,Cl)_2$	0.30	0.60	0.53	0.58	0.65	0.69	0.60	0.62	1.21	0.57	0.89	0.77	0.70
Total	92.64	94.25	94.42	95.13	96.36	94.53	96.68	94.22	92.47	89.16	90.34	91.27	89.77
(Na + K)/Al	4.32	8.87	8.37	7.24	7.24	7.91	7.17	6.94	5.99	3.79	3.37	3.85	3.54

Symbols: Gl—glass; Fl—fluorite; g—gas bubble. n—number of analyses.

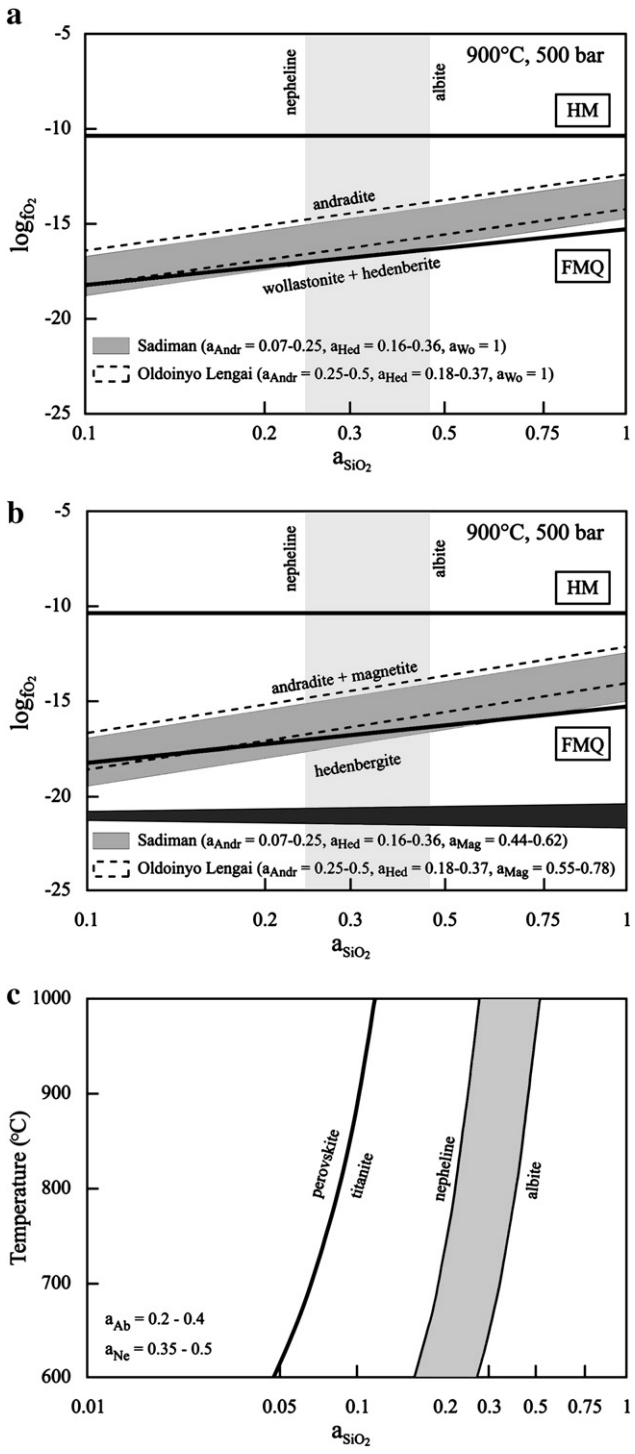

Fig. 12. T–f_{O_2}–a_{SiO_2} diagrams for the Sadiman rocks. (a–b) $\log f_{O_2}$–a_{SiO_2} conditions for the Sadiman rocks compared to similar rocks from Oldoinyo Lengai as derived from equilibria (3) and (4). The black field in diagram (b) represents the estimated calculation error. (c) T–a_{SiO_2} conditions for the Sadiman rocks as derived from equilibria (1) and (2).

factors in their formation. Our mineralogical data for the Sadiman nephelinites (in particular the core–mantle–rim relationships in clinopyroxene; reaction rims around wollastonite phenocrysts; presence of different magnetite microphenocrysts; and replacement reactions between perovskite, titanite, schorlomite, götzenite and aenigmatite (Figs. 4, 6–7) also point to a xenocrystic origin of some crystals (at least for clinopyroxene and magnetite), and disequilibrium conditions of mineral crystallization.

The Sadiman nephelinites are characterized by significant variations in the content of phenocryst minerals, the nephelinites ranging from crystal-rich porphyritic to crystal-poor aphyric varieties (Zaitsev et al., 2011). This range is reflected in variations in the contents of the major components, e.g. SiO_2, Al_2O_3, CaO, Na_2O and K_2O (Fig. 9, Table 3). Despite the differences in mineral assemblage and major-element geochemistry, the studied nephelinites display similar trace element contents, with the exception of the wollastonite nephelinite, which is slightly enriched in trace elements. The nephelinites show a typical "nephelinitic" pattern of trace elements in a primitive mantle-normalized diagram (Fig. 10) (e.g., Klaudius and Keller, 2006; Le Bas, 1987): strong enrichment in Rb, Ba, Th, U, Nb and Pb (135–405 times relatively to PM) and to a lesser degree in Ta and Sr (72–163 times relatively to PM) with clear negative P and Ti anomalies.

Concentrations of these elements in the nephelinites are also higher compared to average ocean island basalts (OIB) (Fig. 10). Several petrological and geochemical studies of volcanic rocks from northern Tanzania suggest involvement of an OIB-like mantle source in the generation of primary melts in this area (see review in Dawson, 2008), but the observed enrichment of some incompatible elements over OIB probably indicates interaction of primary asthenospheric melts with an enriched lithospheric component (Neukirchen et al., 2010 and references therein).

Concentrations of La, Ce and Pr in the nephelinites are higher compared to OIB, whereas the other REE are at a similar level (Fig. 10). On a chondrite-normalized plot, the REE patterns are identical for all samples (Fig. 10) with prominent LREE enrichments ($(La/Sm)_{CN}$ ratio of 7.9–9.9) and relatively flat heavy REE distributions ($(Ho/Lu)_{CN}$ ratio of 1.3–1.5).

Variations in the mineralogy and major elements contents do not significantly affect incompatible element ratios which have relatively narrow ranges, e.g. Zr/Hf = 44.4–53.8, Zr/Nb = 1.7–2.6, La/Nb = 0.7–0.8, Th/U = 3.6–7.3, Ce/Pb = 6.8–9.4.

In recent studies of volcanic complexes from the Crater Highland area, including Sadiman (Mollel, 2007; Mollel et al., 2011), the low Ce/Pb ratio (<20) observed in some evolved rocks was interpreted as an indicator of possible crustal contamination with reference to the study of East African Rift basalts by Furman (2007). However, Mollel et al. (2009) also suggested that the Ce/Pb ratio could not be an obvious indicator of crustal contamination in regions, including northern Tanzania, where the mantle source rock was metasomatically modified (e.g. Dawson and Smith, 1988).

Available data for nephelinites from northern Tanzania show that all evolved nephelinites have low Ce/Pb ratios, with values ranging from 4.5 to 8.4 at Oldoinyo Lengai (Klaudius and Keller, 2006), from 6.3 to 9.3 at Kerimasi (Zaitsev, unpubl. data) and from 5.5 to 11.4 in lava flows of the western escarpment of the Lake Natron area (Neukirchen et al., 2010). A study of primary melt inclusions from the Oldoinyo Lengai combeite–wollastonite nephelinite revealed a very high Pb content in inclusion glasses (60–155 ppm), with a Ce/Pb ratio between 3.3 and 4.2 (Sharygin et al., 2012-this issue). We suggest that relative Pb enrichment of the nephelinites could be related to Pb accumulation during fractional crystallization processes.

7.3. Melt inclusions in nepheline

Bulk rock analyses of the Sadiman nephelinites (Table 3) show that these rocks could not have crystallized from a primary mantle melt, but that they represent the composition of a highly differentiated and partially crystal contaminated melt. The evolved nature of the Sadiman melt(s) is also supported by data from primary glassy inclusions in liquidus nepheline (Fig. 11). The glass is peralkaline (AI = 3.4–8.9) and silica-rich (55.7–58.1 wt.% SiO_2) with low magnesium contents (0.2–0.4 wt.% MgO; Table 5). A notable feature of this glass is the low potassium content (0.5–0.9 wt.% K_2O, rarely up to 5 wt.%), whereas other elements are present at similar concentration

levels found in glasses from Oldoinyo Lengai inclusions in nephelinites (Mitchell, 2009; Sharygin et al., 2012-this issue).

However, unlike Oldoinyo Lengai inclusions, no carbonate and chloride phases were found in the melt inclusions in any of the studied Sadiman samples. Instead, fluorite is a common component in these inclusions, forming euhedral to subhedral crystals (Fig. 11). Fluorine is also found in the glass (0.5–2.4 wt.% F, Table 5), some daughter phases of inclusions (fluorcanasite—3.0–4.9 wt.% F, potassicarfvedsonite —0.2–1.3 wt.% F) and nephelinites contain up to 0.25 wt.% F in the bulk composition (Table 3). Fluorite as a separate mineral phase was not observed as either pheno- or microphenocrysts in the nephelinites, but fluorine is present in apatite, titanite, götzenite and delhayelite-like mineral. Enrichment of melt inclusions in fluorine was also observed in the inclusions of Oldoinyo Lengai nephelinites, where fluorite is commonly present both as a daughter phase in glass of partly crystallized inclusions and as a component of carbonate globules, and the silicate glass contains between 0.9 and 2.3 wt.% F (Sharygin et al., 2012-this issue).

Heating experiments on melt inclusions indicate homogenization temperatures of about 1000–1100 °C for nepheline-, clinopyroxene- and wollastonite-hosted inclusions and up to 1200 °C for those in titanite and apatite. These homogenization temperatures are very similar to those in phenocryst minerals from the Oldoinyo Lengai nephelinites (Sharygin et al., 2012-this issue) and to the lava temperature, 1100 ± 30 °C, of the active nephelinitic Nyiragongo volcano (Platz et al., 2004; Tazieff, 1984).

7.4. Quantitative constraints on intensive parameters for nephelinites

Based on the observed mineral assemblages (Table 1) and the mineral textures (Figs. 2, 4, 6–8), several phase equilibria were identified which, in principle, would allow to constrain the T–f_{O_2}–a_{SiO_2} evolution of the Sadiman nephelinites, if the complete thermodynamic data were available:

$$\begin{array}{l} CaTiO_3 + SiO_2 = CaTiSiO_5 \\ Pv + SiO_2 = Tit \end{array} \quad (1)$$

$$\begin{array}{l} NaAlSiO_4 + 2SiO_2 = NaAlSi_3O_8 \\ Ne + 2SiO_2 = Ab \end{array} \quad (2)$$

$$\begin{array}{l} 3Ca_3Fe_2(SiO_4)_3 + 2Fe_3O_4 + 9SiO_2 = 9CaFeSi_2O_6 + 4O_2 \\ 3Andr + 2Mt + 9SiO_2 = 9Hed + 4O_2 \end{array} \quad (3)$$

$$\begin{array}{l} 2Ca_3Fe_2(SiO_4)_3 + 4SiO_2 = 2CaSiO_3 + 4CaFeSi_2O_6 \\ 2Andr + 4SiO_2 = 2Woll + 4Hed \end{array} \quad (4)$$

$$2Tit + O_2 + Hed = 2Schorl + 6SiO_2 \quad (5)$$

$$Tit + 18SiO_2 + 8Mt + 12Aeg = 6Hed + 6Aen + 7O_2 \quad (6)$$

$$\begin{array}{l} Schorl + 24HF + 6O_2 + 12Ab + 39Hed \\ \quad = 6Grs + 6Gtn + 75SiO_2 + 15Mt + 12H_2O \end{array} \quad (7)$$

Due to the lack of thermodynamic data for schorlomite, aenigmatite and götzenite, equilibria (5)–(7) can be interpreted qualitatively only. Equilibria (1)–(4) were calculated using the GEOCALC software of Berman et al. (1987) and Liebermann and Petrakakis (1990) with the database of Berman (1988). Thermodynamic data for perovskite and titanite were taken from Robie and Hemingway (1995). End-member component activities were calculated using the solution models of Fuhrman and Lindsley (1988) for feldspar, Andersen et al. (1993) for magnetite, the models of Green et al. (2007) and Wood (1979) for clinopyroxene and a mixing-on-site model for nepheline. The activity of andradite was calculated after Cosca et al. (1986) and by using a mixing-on-site model. Wollastonite, titanite and perovskite were treated as pure phases. Unit activity of SiO_2 was referred to the standard state of pure SiO_2 phase at P and T and f_{O_2} values are expressed in log units relative to the fayalite–magnetite–quartz buffer (FMQ). Since the mineral phases show chemical zonation, we used the full range of calculated end member activities to perform the quantitative estimations for f_{O_2} and a_{SiO_2}. As suitable mineral barometers are lacking in the Sadiman rocks, we performed the f_{O_2} calculations for a pressure of 500 bars. Calculating the same phase equilibria for 1 bar, however, does not result in significant changes for f_{O_2} relative to the FMQ buffer, although the absolute values change.

Only very few nepheline compositions seem to have retained their high-temperature composition (Fig. 3) and the data show a general trend of decreasing nepheline component with decreasing SiO_2 component, which is believed to indicate sub-solidus re-equilibration (e.g., Marks et al., 2008; Powell, 1978). The highest temperatures preserved in the nepheline analyses from nephelinites reach 800 °C, with one analysis from a phonolite sample exceeding 1000 °C. Combined with the melt inclusion data (Table 4) we estimate around 900 °C as the final equilibration temperature between phenocryst and microphenocryst phases, and used this temperature for calculating the a_{SiO_2}–f_{O_2} diagrams (Fig. 12a–b). Nevertheless, we explored the effect of temperature variations on the f_{O_2}-dependent calculated phase equilibria (3) and (4). The net effect is a shift to higher f_{O_2} values (relative to FMQ) for lower temperatures. This deviation increases with increasing a_{SiO_2}. The total relative difference for calculations between 800 °C and 1000 °C is about 0.4 log units for $a_{SiO_2} = 0.1$ and about 1.4 log units for $a_{SiO_2} = 1$.

According to reaction (1), the presence or absence of perovskite provides important constraints on silica activity. Perovskite is an early liquidus phase, and in some samples it is overgrown by titanite. Titanite itself occurs as euhedral grains in textural equilibrium with nepheline, garnet, clinopyroxene ± wollastonite ± sanidine ± magnetite. This implies that initial silica activity in these rocks was very low and increased during the crystallization of the main phenocryst assemblage to values > 0.1 (Fig. 12c). For sanidine-bearing nephelinites, equilibrium (2) constrains a_{SiO_2} to values between 0.25 and 0.43, which may also serve as a maximum $aSiO_2$ estimate for feldspar-free samples.

In nephelinites, oxygen fugacity is buffered by phenocryst-involving reactions (3)–(5), which allow us to estimate liquidus to sub-liquidus conditions for the investigated samples. However, due to the absence of thermodynamic data for schorlomite, only reactions (3) and (4) can be used for quantitative constraints.

The wollastonite-involving and magnetite-absent reaction (4) applies to nephelinite II, whereas reaction (3) is applicable to nephelinites I, III and IV. However, both reactions lie close to the FMQ buffer reaction and yield a similar f_{O_2} range between ΔFMQ = −0.5 and +2, for silica activities between 0.25 and 0.43, as constrained by reaction (2).

The calculated range of f_{O_2} values for the Sadiman nephelinites is relatively broad, which is because of the above-mentioned chemical zonation in the major phenocryst phases. The results of similar calculations for mineralogically similar nephelinites from the nearby Oldoinyo Lengai volcano using published mineral data of Dawson (1998) and assuming again 900 °C as equilibration temperature between phenocryst and microphenocryst phases (Sharygin et al., 2012-this issue) are shown in Fig. 12a–b for comparison. Although they show considerable overlap, it seems that the Lengai nephelinites are even more oxidized than the Sadiman nephelinites. Obviously, the garnet-bearing Sadiman and Oldoinyo Lengai nephelinites equilibrated at relatively oxidizing conditions (above the FMQ buffer), which are very different from the generally strongly reducing conditions (below the FMQ buffer) indicated by peralkaline trachytes and pantellerites from the Kenyan part of the Gregory Rift (e.g., Macdonald et al., 2011; Ren et al., 2006) and elsewhere (e.g., White et al., 2005).

This is a particularly important observation as some of the evolved silica-rich (SiO_2 > 54 wt.%) volcanic rocks from the Gregory rift are interpreted, on the basis of rock chemistry and Sr–Nd isotope characteristics,

as being influenced by significant crustal assimilation processes additional to fractional crystallization (AFC processes; Kabeto et al., 2001), which is consistent with the quartz-bearing character of some of the lavas.

On the other hand, mineralogical, geochemical and isotopic studies of the nephelinites as well as associated carbonatites from East Africa (e.g. Bell, 1998; Bell and Dawson, 1995; Bell and Peterson, 1991; Bell and Tilton, 2001; Faure, 2001; Paslick et al., 1996; Peterson, 1989; Simonetti and Bell, 1994) suggest that the nephelinites seem to be relatively uncontaminated by crustal material. Instead, observed xenocrystic material in nephelinites and variable Sr–Nd–Pb isotopic ratios can be explained by mixing of different magma batches derived from a geochemically heterogeneous mantle source, mantle contamination and assimilation of previously crystallized plutonic rocks, e.g. ijolites.

Redox conditions significantly above the FMQ buffer were also reported for mineralogically similar cumulate rocks (garnet-bearing pyroxenites) from the Tamazeght complex, Morocco (Marks et al., 2008) where it was proposed that andradite–schorlomite crystallization in silicate rocks is favored by relatively oxidizing conditions, the assemblage titanite + magnetite represents intermediate f_{O_2} conditions whereas relatively low f_{O_2} will enhance the relative stability of clinopyroxene and ilmenite. Spatially associated with these rocks are garnet-free but titanite-, magnetite-, and ilmenite-bearing monzonitic to gabbroic rocks, for which relatively reducing conditions (down to about $\Delta FMQ = -2$) were derived (Marks et al., 2008). Importantly, the Tamazeght Complex contains genetically related calcite and dolomite carbonatites (Marks et al., 2009). If one postulates a nephelinitic parental melt for the oxidized Tamazeght rocks (Bouabdli et al., 1988; Kchit, 1990; Marks et al., 2008), the similarities of the garnet-bearing, oxidized rocks associated with carbonatites from Tamazeght with the mineralogical observations from Sadiman and Oldoinyo Lengai are striking. In that sense, the Sadiman nephelinites might be close to a carbonatitic evolution trend and an important pre-requisite for carbonatite formation appears to be the existence of relatively oxidized mantle melts.

8. Conclusions

The results of the present study of the Sadiman volcano combined with previously published data discussed above lead to following conclusions:

1 – Nephelinite lavas and phonolitic tuffs are the principle rock types at the Sadiman volcano, while phonolite lavas are very rare rocks. Available to date geological, mineralogical and geochemical data do not support the occurrence of melilite-bearing rocks and carbonatites (or natrocarbonatites) at Sadiman. The occurrence of ijolitic rocks indicates the presence of a plutonic complex beneath Sadiman.

2 – The nephelinites possess mineralogical and geochemical characteristics that are similar to nephelinites from the Shombole, Kerimasi and Oldoinyo Lengai carbonatitic volcanoes. However, primary carbonate mineral(s), known in nephelinites from the Gregory rift (e.g. calcite in Shombole, calcite and nyerereite in Kerimasi, and nyerereite and gregoryite in Oldoinyo Lengai) were not found in the Sadiman nephelinites. The latter are highly evolved alkaline to peralkaline rocks, crystallized from a differentiated and partly crystal contaminated melt, and some of the nephelinites are transitional to phonolites.

3 – Heating experiments, phase assemblages and the chemical composition of melt inclusions in nepheline from the Sadiman nephelinites indicate high temperatures during crystallization of the phenocryst assemblage (>1000 °C) and enrichment of the melt in volatile components, particularly in fluorine. Available data for primary melt inclusions in the Sadiman (this study), Oldoinyo Lengai (Mitchell, 2009; Sharygin et al., 2012-this issue) and Mosonik nephelinites (Bazarova et al., 1975; Sharygin, unpubl. data) show the presence of fluorite as an individual phase and silicate–natrocarbonatite or silicate-CaF_2 liquid immiscibility. In the case of Sadiman, the silicate-CaF_2 liquid immiscibility is clearly seen in nepheline-hosted inclusions during heating. However, during the crystallization of nephelinites this process is hidden or "invisible" due to the formation of other F-bearing minerals (titanite, apatite, götzenite, etc.) instead of fluorite.

4 – Mineral assemblages and mineral chemistry of the Sadiman nephelinites suggest their crystallization under relatively oxidizing conditions (above the FMQ buffer), which differ from the reducing conditions reported earlier for trachytic and pantelleritic rocks from the Gregory rift (Macdonald et al., 2011; Ren et al., 2006). Redox conditions above the FMQ buffer seem to be typical of garnet-bearing nephelinites and might thus indicate a relatively oxidized mantle reservoir, which seems to be a prerequisite for carbonatite formation as observed for example at Oldoinyo Lengai and in the Tamazeght complex (Morocco).

Acknowledgments

We thank Dr. Mike Kobrick (Project Scientist, Shuttle Radar Topography Mission, Jet Propulsion Lab, Pasadena, USA) for permission to publish Fig. 1a, which was generated by Dr. Robert Crippen. We thank Catherine Unsworth for help with the ICP-AES analyses. We are grateful to Nelson Eby and two anonymous reviewers for constructive comments. This research was supported by the Alexander von Humboldt Stiftung (Germany), St. Petersburg State University, the Natural History Museum (UK) and the Russian Foundation for Basic Research (grant 11-05-00875).

Supplementary text and data

Supplementary text and data to this article can be found online at doi:10.1016/j.lithos.2012.03.001.

References

Andersen, D.J., Lindsley, D.H., Davidson, P.M., 1993. QUILF: a PASCAL program to assess equilibria among Fe–Mg–Mn–Ti oxides, pyroxenes, olivine, and quartz. Computers and Geosciences 19, 1333–1350.

Bagdasaryan, G.P., Gerasimovskiy, V.I., Polyakov, A.I., Gukasyan, R.K., Vernadskiy, V.I., 1973. Age of volcanic rocks in the rift zones of East Africa. Geochemistry International 10, 66–71.

Bazarova, T. Yu., Bakumenko, I.T., Kostyuk, V.P., Panina, L.I., Sobolev, V.S., Chepurov, A.I., 1975. Magmatic Crystallisation Based on the Study of Melt Inclusions. Nauka, Novosibirsk. (in Russian).

Bell, K., 1998. Radiogenic isotope constraints on relationships between carbonatites and associated silicate rocks—a brief review. Journal of Petrology 39, 1987–1996.

Bell, K., Peterson, T.D., 1991. Nd and Sr isotope systematics of Shombole volcano, East Africa, and the links between nephelinites, phonolites, and carbonatites. Geology 19, 582–585.

Bell, K., Dawson, J.B., 1995. Nd and Sr isotope systematics of the active carbonatite volcano, Oldoinyo Lengai. Carbonatite Volcanism: Oldoinyo Lengai and the Petrogenesis of Natrocarbonatites. : In: Bell, K., Keller, J. (Eds.), IAVCEI Proceedings in Volcanology, 4. Springer, Berlin, pp. 100–112.

Bell, K., Tilton, G.R., 2001. Nd, Pb and Sr isotopic compositions of East African carbonatites: evidence for mantle mixing and plume inhomogeneity. Journal of Petrology 42, 1927–1945.

Berger, J., Ennih, N., Mercier, J.-C.C., Liégeois, J.-P., Demaiffe, D., 2009. The role of fractional crystallization and late-stage peralkaline melt segregation in the mineralogical evolution of Cenozoic nephelinites/phonolites from Saghro (SE Morocco). Mineralogical Magazine 73, 59–82.

Belousov, V.V., Gerasimovski, V.I., Goryachev, A.V., Dobrovolski, V.V., Kapitsa, A.P., Logachev, A.V., Milanovski, E.E., Poliakov, A.I., Rikunov, L.N., Sedov, V.V., 1974. East-African Rift System, Vol. 1–3. Nauka, Moscow. (in Russian).

Berman, R., 1988. Internally consistent thermodynamic data for minerals in the system Na_2O–K_2O–CaO–MgO–FeO–Fe_2O_3–Al_2O_3–SiO_2–TiO_2–H_2O–CO_2. Journal of Petrology 29, 445–522.

Berman, R.G., Brown, T.H., Perkins, E.H., 1987. Geo-Calc; a software for calculation and display of P–T–X phase diagrams. American Mineralogist 72, 861–862.

Bouabdli, A., Dupuy, C., Dostal, J., 1988. Geochemistry of Mesozoic alkaline lamprophyres and related rocks from the Tamazert massif, High Atlas, (Morocco). Lithos 22, 43–58.
Church, A.A., 1996. The petrology of the Kerimasi carbonatite volcano and the carbonatites of Oldoinyo Lengai with a review of other occurrences of extrusive carbonatites. Ph.D. Dissertation, University of London.
Cosca, M.A., Moecher, D.P., Essene, E.J., 1986. Activity-composition relations for the join grossular-andradite and application to calc-silicate assemblages. Abstracts with Programs—Geological Society of America 18, 572.
Dawson, J.B., 1998. Peralkaline nephelinite–natrocarbonatite relationships at Oldoinyo Lengai, Tanzania. Journal of Petrology 39, 2077–2094.
Dawson, J.B., 2008. The Gregory rift Valley and Neogene–Recent volcanoes of northern Tanzania. Geological Society Memoir No. 33. Geological Society, London.
Dawson, J.B., Smith, J.V., 1988. Metasomatised and veined upper-mantle xenoliths from Pello Hill, Tanzania: evidence for anomalously light mantle beneath the Tanzanian sector of the East African Rift Valley. Contributions to Mineralogy and Petrology 100, 510–527.
Dawson, J.B., Smith, J.V., Jones, A.P., 1985. A comparative study of bulk rock and mineral chemistry of olivine melilitites and associated rocks from East and South Africa. Neues Jahrbuch für Mineralogie, Abhandlungen 152, 143–175.
Faure, G., 2001. Origin of Igneous Rocks. The Isotopic Evidence. Springer, Berlin. 496 pp.
Ferrat, M., Weiss, D.J., Strekopytov, S., 2012. A single procedure for the accurate and precise quantification of the rare earth elements, Sc, Y, Th and Pb in dust and peat for provenance tracing in climate and environmental studies. Talanta. http://dx.doi.org/10.1016/j.talanta.2012.01.052.
Foster, A., Ebinger, C., Mbede, E., Rex, D., 1997. Tectonic development of the northern Tanzanian sector of the east African rift System. Journal of the Geological Society of London 154, 689–700.
Fuhrman, M.L., Lindsley, D.H., 1988. Ternary-feldspar modeling and thermometry. American Mineralogist 73, 201–205.
Furman, T., 2007. Geochemistry of East African Rift basalts: an overview. Journal of African Earth Sciences 48, 147–160.
Green, E., Holland, T., Powell, R., 2007. An order–disorder model for omphacitic pyroxenes in the system jadeite–diopside–hedenbergite–acmite, with application to eclogitic rocks. American Mineralogist 92, 1181–1189.
Hamilton, D.L., 1961. Nephelines as crystallisation temperature indicators. Journal of Geology 69, 321–329.
Harrison, T. (Ed.), 2011a. Paleontology and Geology of Laetoli: Human Evolution in Context Volume 1: Geology, Geochronology, Paleoecology and Paleoenvironment. Springer, Dordrecht.
Harrison, T., 2011b. Laetoli revisited: renewed paleontological and geological investigations at localities on the Eyasi plateau in northern Tanzania. In: Harrison, T. (Ed.), Paleontology and Geology of Laetoli: Human Evolution in Context Volume 1: Geology, Geochronology, Paleoecology and Paleoenvironment. Springer, Dordrecht, pp. 1–15.
Hay, R.L., 1976. Geology of the Olduvai Gorge. University of California Press, Berkeley.
Hay, R.L., 1978. Melilitite–carbonatite tuffs in the Laetoli Beds of Tanzania. Contributions to Mineralogy and Petrology 67, 357–367.
Hay, R.L., 1987. Geology of the Laetoli area. In: Leakey, M.D., Harris, J.M. (Eds.), Laetoli, a Pliocene Site in Northern Tanzania. Clarendon Press, Oxford, pp. 23–47.
Hezel, D.C., Schlüter, J., Kallweit, H., Jull, A.J.T., Al Fakeer, O.Y., Al Shamsi, M., Strekopytov, S., 2011. Meteorites from the United Arab Emirates: description, weathering and terrestrial ages. Meteoritics and Planetary Sciences 46, 327–336.
James, T.C., 1966. The carbonatites of Tanganyika: a phase of continental-type volcanism. Ph.D. Dissertation, Imperial College.
Kabeto, K., Sawada, Y., Iizumi, S., Wakatsuki, T., 2001. Mantle sources and magma–crust interactions in volcanic rocks from the northern Kenya rift: geochemical evidence. Lithos 56, 111–139.
Keller, J., Zaitsev, A.N., Wiedenmann, D., 2006. Primary magmas at Oldoinyo Lengai: the role of olivine melilitites. Lithos 91, 150–172.
Kchit, A., 1990. Le plutonisme alcalin du Tamazert, Haut Atlas de Midelt (Maroc), Petrologie et Structurologie. Unpublished thesis, Univ. Paul Sabatier, Toulouse.
Klaudius, J., Keller, J., 2006. Peralkaline silicate lavas at Oldoinyo Lengai, Tanzania. Lithos 91, 173–190.
Korobeinikov, A.N., Laajoki, K., 1994. Petrological aspects of the evolution of clinopyroxene composition in the intrusive rocks of the Lovozero alkaline massif. Geochemistry International 31, 69–76.
Larsen, L.M., 1976. Clinopyroxenes and coexisting mafic minerals from the alkaline Ilímaussaq intrusion, south Greenland. Journal of Petrology 17, 258–290.
Le Bas, M.J., 1987. Nephelinites and carbonatites. Alkaline Igneous Rocks: In: Fitton, J.G., Upton, B.G.J. (Eds.), Geological Society Special Publication No. 30, pp. 53–83.
Leakey, M.D., Hay, R.L., 1979. Pliocene footprints in the Laetolil Beds at Laetoli, northern Tanzania. Nature 278, 317–323.
Liebermann, J., Petrakakis, K., 1990. TWEEQU thermobarometry, analysis of uncertainties and applications to granulites from western Alaska. The Canadian Mineralogist 29, 857–887.
Macdonald, R., Bagiński, B., Leat, P.T., White, J.C., Dzierżanowski, P., 2011. Mineral stability in peralkaline silicic rocks: information from trachytes of the Menengai volcano, Kenya. Lithos 125, 553–568.
Mann, U., Marks, M.A.W., Markl, G., 2006. Influence of oxygen fugacity on mineral compositions in peralkaline melts: the Katzenbuckel volcano, Southwest Germany. Lithos 91, 262–285.
Markl, G., Marks, M., Schwinn, G., Sommer, H., 2001. Phase equilibrium constraints on intensive crystallization parameters of the Ilimaussaq Complex, South Greenland. Journal of Petrology 42, 2231–2258.
Marks, M., Markl, G., 2001. Fractionation and assimilation processes in the alkaline augite syenite unit of the Ilimaussaq intrusion, South Greenland, as deduced from phase equilibria. Journal of Petrology 42, 1947–1969.
Marks, M.A.W., Schilling, J., Coulson, I.M., Wenzel, T., Markl, G., 2008. The alkaline–peralkaline Tamazeght complex, High Atlas Mountains, Morocco: mineral chemistry and petrological constraints for derivation from a compositionally heterogeneous mantle source. Journal of Petrology 49, 1097–1131.
Marks, M.A.W., Neukirchen, F., Markl, G., Vennemann, T., 2009. Textural, chemical, and isotopic effects of late-magmatic carbonatitic fluids in the carbonatite–syenite Tamazeght complex, High Atlas Mountains, Morocco. Mineralogy and Petrology 97, 23–42.
Mitchell, R.H., 2009. Peralkaline nephelinite–natrocarbonatite immiscibility and carbonatite assimilation at Oldoinyo Lengai, Tanzania. Contributions to Mineralogy and Petrology 158, 589–598.
Mitchell, R.H., Platt, R.G., 1982. Mineralogy and petrology of nepheline syenites from the Coldwell alkaline complex, Ontario, Canada. Journal of Petrology 23, 186–214.
Mollel, G.F., 2007. Petrochemistry and geochronology of Ngorongoro Volcanic Highland Complex (NVHC) and its relationship to Laetoli and Olduvai Gorge, Tanzania. Ph.D. Dissertation, Rutgers University.
Mollel, G.F., Swisher III, C.C., Feigenson, M.D., Carr, M.J., 2008. Geochemical evolution of Ngorongoro Caldera, Northern Tanzania: implications for crust-magma interaction. Earth and Planetary Science Letters 271, 337–347.
Mollel, G.F., Swisher, C.C., McHenry, L.J., Feigenson, M.D., Carr, M.J., 2009. Petrogenesis of basalt-trachyte lavas from Olmoti crater, Tanzania. Journal of African Earth Sciences 54, 127–143.
Mollel, G.F., Swisher, C.C., Feigenson, M.D., Carr, M.J., 2011. Petrology, geochemistry and age of Satiman, Lemagurut and Oldeani: sources of the volcanic deposits of the Laetoli area. In: Harrison, T. (Ed.), Paleontology and Geology of Laetoli: Human Evolution in Context Volume 1: Geology, Geochronology, Paleoecology and Paleoenvironment. Springer, Dordrecht, pp. 99–119.
Mutakyahwa, M., 1997. Mineralogy of the Wembere-Manonga formation, Manonga Valley, Tanzania, and possible provenance of the sediments. In: Harrison, T. (Ed.), Neogene Paleontology of the Manonga Valley, Tanzania. Plenum, New York, pp. 67–78.
Naumov, V.B., Polyakov, A.I., Romanchev, B.P., 1972. Thermobarometric evidence on the crystallization conditions of east African rift-zone volcanic rocks. Geochemistry International 9 (3), 427–431.
Neukirchen, F., Finkenbein, T., Keller, J., 2010. The Lava sequence of the East African Rift escarpment in the Oldoinyo Lengai—Lake Natron sector, Tanzania. Journal of African Earth Sciences 58, 734–751.
Paslick, C., Halliday, A., James, D., Dawson, J.B., 1995. Enrichment of the continental lithosphere by OIB melts: isotopic evidence from the volcanic province of northern Tanzania. Earth and Planetary Science Letters 130, 109–126.
Paslick, C.R., Halliday, A.N., Lange, R.A., James, D., Dawson, J.B., 1996. Indirect crustal contamination: evidence from isotopic and chemical disequilibria in minerals from alkali basalts and nephelinites from northern Tanzania. Contributions to Mineralogy and Petrology 125, 277–292.
Pekov, I.V., Zubkova, N.V., Chukanov, N.V., Sharygin, V.V., Pushcharovsky, D. Yu., 2009. Crystal chemistry of delhayelite and hydrodelhayelite. Doklady Earth Sciences 428, 1216–1221.
Peterson, T.D., 1989. Peralkaline nephelinites. I. Comparative petrology of Shombole and Oldoinyo L'engai, East Africa. Contributions to Mineralogy and Petrology 101, 458–478.
Pickering, R., 1964. Endulen. Tanzania Geological Survey Quarter Degree Sheet 52.
Platz, Th., Foley, S.F., André, L., 2004. Low-pressure fractionation of the Nyiragongo volcanic rocks, Virunga Province, D.R. Congo. Journal of Volcanology and Geothermal Research 136, 269–295.
Powell, M., 1978. The crystallisation history of the Igdlerfigssalik nepheline syenite intrusion, Greenland. Lithos 11, 99–120.
Redhammer, G.J., Roth, G., Topa, D., Amthauer, G., 2008. Synthetic aenigmatite analog $Na_2(Mn_{5.26}Na_{0.74})Ge_6O_{20}$: structure and crystal chemical considerations. Acta Crystallographica C64, 21–26.
Ren, M., Omenda, P.A., Anthony, E.Y., White, J.C., Macdonald, R., Bailey, D.K., 2006. Application of the QUILF thermobarometer to the peralkaline trachytes and pantellerites of the Eburru volcanic complex, East African Rift, Kenya. Lithos 91, 109–124.
Robie, R.A., Hemingway, B.S., 1995. Thermodynamic properties of minerals and related substances at 298.15 K and 1 bar (105 Pascals) pressure and at higher temperatures. U.S. Geological Survey Bulletin 2131, 461.
Sharygin, V.V., Kamenetsky, V.S., Zaitsev, A.N., Kamenetsky, M.B., 2012. Silicate–natrocarbonatite liquid immiscibility in 1917 eruption combeite–wollastonite nephelinite, Oldoinyo Lengai Volcano, Tanzania: Melt inclusion study. Lithos 152, 23–39 (this issue).
Simonetti, A., Bell, K., 1994. Nd, Pb and Sr isotopic data from the Napak carbonatite–nephelinite centre, eastern Uganda: an example of open-system crystal fractionation. Contributions to Mineraloly and Petrology 115, 356–366.
Sobolev, A.V., Slutsky, A.B., 1984. Composition and crystallization conditions of initial melt of the Siberian meimechites in relation to the general problem of the ultrabasic magmas. Soviet Geology and Geophysics 25, 93–104.
Sun, S.-s., McDonough, W.F., 1989. Chemical and isotopic systematics of oceanic basalts: implications for mantle composition and processes. Geological Society, London, Special Publications 42, 313–345.
Tazieff, H., 1984. Mt. Niragongo: renewed activity of the lava lake. Journal of Volcanology and Geothermal Research 20, 267–280.
Vuorinen, J.H., Hålenius, U., Whitehouse, M.J., Mansfeld, J., Skelton, A.D.L., 2005. Compositional variations (major and trace elements) of clinopyroxene and Ti-andradite from pyroxenite, ijolite and nepheline syenite, Alnö Island, Sweden. Lithos 81, 55–77.

White, J.C., Ren, M., Parker, D.F., 2005. Variation in mineralogy, temperature, and oxygen fugacity in a suite of strongly peralkaline lavas and tuffs, Pantelleria, Italy. The Canadian Mineralogist 43, 1331–1347.

Wood, B.J., 1979. Activity-composition relationships in $Ca(Mg,Fe)Si_2O_6$–$CaAl_2SiO_6$ clinopyroxene solid solution. American Journal of Science 279, 854–875.

Wiedenmann, D., Keller, J., Zaitsev, A.N., 2010. Melilite-group minerals at Oldoinyo Lengai, Tanzania. Lithos 118, 112–118.

Wiedenmann, D., Zaitsev, A.N., Britvin, S.N., Krivovichev, S.V., Keller, J., 2009. Alumoåkermanite, $(Ca, Na)_2(Al, Mg, Fe^{2+})(Si_2O_7)$, a new mineral from the active carbonatite–nephelinite–phonolite volcano Oldoinyo Lengai, northern Tanzania. Mineralogical Magazine 73, 373–384.

Woolley, A.R., 2001. Alkaline Rocks and Carbonatites of the World. Part 3: Africa. The Geological Society, London.

Zaitsev, A.N., 2010. Nyerereite from calcite carbonatite of Kerimasi volcano, northern Tanzania. Geology of Ore Deposits 52 (7), 630–640.

Zaitsev, A.N., Williams, C.T., Britvin, S.N., Kuznetsova, I.V., Spratt, J., Petrov, S.V., Keller, J., 2010. Kerimasite, $Ca_3Zr_2(Fe^{3+}{}_2Si)O_{12}$, a new garnet from carbonatites of Kerimasi volcano and surrounding explosion craters, northern Tanzania. Mineralogical Magazine 74, 841–858.

Zaitsev, A.N., Wenzel, T., Spratt, J., Williams, T.C., Strekopytov, S., Sharygin, V.V., Petrov, S.V., Golovina, T.A., Zaitseva, E.O., Markl, G., 2011. Was Sadiman volcano a source for the Laetoli Footprint Tuff? Journal of Human Evolution 61, 121–124.